NEVADA DOT

Safety and Operations of Large-Area Rural/Urban Intermodal Systems
SOLARIS
A Tier 1 university transportation center led by the University of Nevada, Reno.

Final Report
September 2016

Interconversion of Dynamic Modulus to Creep Compliance and Relaxation Modulus: Numerical Modeling and Laboratory Validation

SOLARIS Consortium, Tier 1 University Transportation Center
Center for Advanced Transportation Education and Research
Department of Civil and Environmental Engineering
University of Nevada, Reno
Reno, NV 89557

Rafiqul A. Tarefder, PhD, PE
Associate Director, SOLARIS
Professor, Civil Engineering
University of New Mexico
Albuquerque, NM 87131

DISCLAIMER

RESEARCH PROJECT SUMMARY

1. Report No.	2. Government Accession No.	3. Recipient's Catalog No.

4. Title and Subtitle Interconversion of Dynamic Modulus to Creep Compliance and Relaxation Modulus: Numerical Modeling and Laboratory Validation - Final Report	5. Report Date September, 2016
	6. Performing Organization Code University of New Mexico
7. Author(s): Rafiqul A. Tarefder, and A. S. M. Asifur Rahman	8. Performing Organization Report No. 456-438-Final Report
9. Performing Organization Name and Address University of New Mexico Department of Civil Engineering MSC01 1070 1 University of New Mexico Albuquerque, NM 87131	10. Work Unit No. (TRAIS)
	11. Contract/Grant No. 456-438
12. Sponsoring Agency Name and Address SOLARIS Consortium, Tier 1 University Transportation Center Center for Advanced Transportation Education and Research Department of Civil and Environmental Engineering University of Nevada, Reno Reno, NV 89557	13. Type of Report and Period Covered Final Report October 1, 2014– June 30, 2016
	14. Sponsoring Agency Code

15. Supplementary Notes The research project is funded by NDOT in cooperation with FHWA.

16. Abstract

Viscoelastic material functions such as time domain functions, such as, relaxation modulus and creep compliance, or frequency domain function, such as, complex modulus can be used to characterize the linear viscoelastic behavior of asphalt concrete in modeling and analysis of pavement structure. Among these, the complex modulus has been adopted in the recent pavement Mechanistic-Empirical (M-E) design software AASHTOWare-ME. However, for advanced analysis of pavement, such as, use of finite element method requires that the complex modulus function to be converted into relaxation modulus or creep compliance functions. There are a number of exact or approximate methods available in the literature to convert complex modulus function to relaxation modulus or creep compliance functions. All these methods (i.e. exact or approximate methods) are applicable for any linear viscoelastic material up to a certain level of accuracy. However, the applicability and accuracy of these interconversion methods for asphalt concrete material were not studied very much in the past and thus question arises if these methods are even applicable in case of asphalt concrete, and if so, what is the precision level of the interconversion method being used. Therefore, to investigate these facts, this study undertaken an effort to validate a numerical interconversion technique by conducting representative laboratory tests. Cylindrical specimens of asphalt concrete were prepared in the laboratory for conducting complex modulus, relaxation modulus, and creep compliance tests at different test temperatures and loading rates. The time-temperature superposition principle was applied to develop broadband linear viscoelastic material functions. A numerical interconversion technique was used to convert complex modulus function to relaxation modulus and creep compliance functions, and hence, the converted relaxation modulus and creep compliance are compared to the laboratory tested relaxation modulus and creep compliance functions. The comparison showed good agreement with the laboratory test data. Toward the end, a statistical evaluation was conducted to determine if the interconverted material functions are similar to the laboratory tested material functions.

17. Key Words Dynamic Modulus, Phase Angle, Relaxation Modulus, Creep Compliance, Interconversion, Asphalt Concrete, Asphalt Pavement	18. Distribution Statement No Restriction

19. Security Classification of the Report None	20. Security Classification of this page None	21. Number of Pages 61	22. Price N/A

TABLE CONTENTS

LIST OF FIGURES

LIST OF TABLES

INTRODUCTION

Dynamic modulus (|*E**|) and creep compliance *D*(*t*) are important input parameters in the mechanistic-empirical (M-E) design and analysis of pavements. In recently developed M-E design of pavement method, the |*E**| of asphalt concrete is used to predict rutting and fatigue cracking of asphalt concrete and *D*(*t*) is primarily used for predicting low temperature cracking of pavements. Currently, both the |*E**| and *D*(*t*) tests are performed separately for using them in M-E design of pavements. The present study is basically an effort to derive *D*(*t*) values of asphalt concrete from |*E**| test data through numerical interconversion. Thus if the study proved to be successful, D(t) testing can be eliminated or at a minimum can be limited/reduced and thereby help implementation of M-E design method in the state of New Mexico.

There are a number of viscoelastic material functions available to characterize the linear viscoelastic (LVE) behavior of asphalt concrete (AC). Some of these are expressed in time domain, such as, relaxation modulus E(t) or creep compliance D(t) and some are expressed in frequency domain, such as, dynamic or complex modulus (|E*|, or E*). The E* of AC material is useful for the implementation of mechanistic-empirical (M-E) analysis and design of pavement [1]. However, time domain LVE material functions of AC may be required for constitutive modeling or finite element application.

The relationships between LVE material functions have a basis in the theory of linear differential and integral equations. Therefore, a source LVE function can be converted into a target LVE function as long as the source function is known over a wide-enough range of time or frequency. Researchers like Hopkins and Hamming [2], Knoff and Hopkins [3], Baumgaertel and Winter [4], Mead [5], Schapery and Park [6], Ramkumar et al. [7], Park and Schapery [8] presented different approaches to convert one linear viscoelastic function to another for polymer materials. Mun et al. [9] gave an interconversion technique to convert frequency-domain LVE functions of AC to time-domain LVE functions. However, in their exact method of interconversion, the details about calculating the time constants (e.g. calculation of retardation times from the relaxation times) are missing. Park and Kim proposed a new approximate interconversion method between E(t) and D(t) of AC [10]. Their scheme is based on the concept of equivalent time which can be determined by rescaling the physical time.

To study the effect of any physical or environmental factors to the LVE material functions of asphalt concrete, application of a valid interconversion technique is always helpful in terms of cost and time. An appropriate interconversion technique can reduce the cost of testing and thus can reduce the study time. Danial et al. (11) studied the effect of aging on viscoelastic properties of asphalt-aggregate mixture, such as creep compliance, relaxation modulus, dynamic modulus and phase angle. In their study the creep compliance testing was performed and the relaxation modulus is predicted through the procedure based on theory of linear viscoelasticity suggested by Kim and Lee (12).

OBJECTIVE

The main objective of this study is to perform representative laboratory tests on various LVE material functions of AC to evaluate the validity of the numerical method employed herein for interconversion of frequency domain complex modulus function to time domain relaxation modulus or creep compliance functions. The linear viscoelastic material functions considered in this study are: time-domain functions such as relaxation modulus E(t), and creep compliance D(t); and frequency-domain function as complex modulus E^* of AC. Toward the end, a statistical evaluation was conducted in this study to determine if the interconverted material functions are similar to the laboratory tested relaxation modulus and creep compliance functions.

The specific objectives include: conduct dynamic modulus (|E*|) testing on selected asphalt mixes collected from actual pavement construction sites in New Mexico, write code based on existing theory or modifying existing theory to convert dynamic modulus data to creep compliance, validate the numerical |E*|-D(t) interconversion results using creep test to be conducted in the laboratory, and conduct relaxation modulus E(t) testing for additional validation.

RESEARCH PROGRAM

In order to achieve the research objective, the activities/tasks completed in the course of this study are: (1) asphalt mix collection and sample preparation, (2) dynamic/complex modulus testing, (3) interconversion of dynamic modulus to creep compliance and relaxation modulus, (4) creep compliance testing and validation of interconversion, and (5) relaxation modulus testing and validation of interconversion.

Task 1: Asphalt Mix Collection and Sample Preparation

Materials

In cooperation with the New Mexico Department of Transportation (NMDOT), a total of four Asphalt Concrete (AC) mixtures were collected from different paving sites in New Mexico. Table 1 shows the Superpave® gradation and the associated asphalt binder Performance Grades (PG) of the collected AC mixtures.

Table 1. Asphalt concrete mixes collected

No	Superpave mix	Binder PG grade
1	SP-III	70-22
2	SP-III	76-22
3	SP-IV	70-22
4	SP-IV	76-22

Preparation of Test Specimens

A Superpave® Gyratory Compactor (SGC) was used to compact loose AC mixtures. Cylindrical AC cores of 150 mm in diameter and 170 mm in height were compacted. The target air void was set at 5.5±0.5 for the finished specimen to avoid possible deviation in test results due to large air void variation. Several trial AC mixes were compacted at the beginning with different weights of loose AC material. The required number of gyrations to reach 170 mm overall height was then noted for each trial AC cores. The compacted samples were then core-drilled and sawed to finished specimens of diameter 100 mm and of height 150 mm. The theoretical maximum specific gravity (G_{mm}) was determined by AASHTO T 209 standard. The bulk specific gravity (G_{mb}) was determined according to the AASHTO T 166 protocol. The loose mix weight corresponding to the air void content of 5.5±0.5 were then used to compact further AC cores. For each AC mixture seven cylindrical specimens were prepared, among which, 3 specimens were prepared for dynamic modulus ($|E^*|$) testing, 2 specimens were prepared for creep compliance ($D(t)$) testing, and another 2 specimens were prepared for relaxation modulus ($E(t)$) testing.

Task 2: Dynamic/Complex Modulus Testing

Laboratory Dynamic/Complex Modulus Testing

Dynamic modulus ($|E^*|$) with Phase Angle (δ) testing of all the mixes has been conducted at five different temperatures of 14, 40, 70, 100 and 130°F (-10, 4.4, 21.1, 37.8, and 54.4 °C) and six different loading frequencies of 0.1, 0.5, 1, 5, 10, and 25 Hz at each temperature. The average of $|E^*|$ and δ of all the mixes were then determined.

Dynamic Modulus Mastercurves

The time-temperature superposition principal (TTSP) was applied to develop $|E^*|$ and δ mastercurves at 70 °F reference temperature. For fitting $|E^*|$ mastercurves the following sigmoid expression was used:

$$\log\left(|E^*|\right) = \delta_{MC} + \frac{\alpha}{1 + e^{\beta + \gamma \log\left(f_r\right)}} . \tag{1}$$

In Eq. (1), f_r is the reduced frequency; δ_{MC} is the minimum modulus value; α is the vertical span of the $|E^*|$ function; $\alpha + \delta_{MC}$ is the maximum value of $|E^*|$; β and γ are the shape parameters. The parameters (e.g. α, β, δ_{MC}, and γ) can be found by fitting laboratory tested $|E^*|$ mastercurve.

Phase Angle Mastercurve

The same temperature-frequency shift factors for $|E^*|$ mastercurve can be used to develop δ mastercurve. The resulting δ mastercurve is expected to be a single smooth curve. For fitting δ mastercurve, following expression is used:

$$\delta\left(f_r\right) = \xi_1 + \xi_2 \log\left(f_r\right) - \xi_3 \, \frac{\pi}{2} \, \alpha\gamma \, \frac{e^{\beta + \gamma \log\left(f_r\right)}}{\left(1 + e^{\beta + \gamma \log\left(f_r\right)}\right)^2} \tag{2}$$

In Eq. (7), $\delta(f_r)$ is the phase angle in radians; f_r is the reduced frequency in Hz; and α, β, and γ are the regression coefficients found by fitting $|E^*|$ function by Eq. (1). ξ_1, ξ_2, and ξ_3 are the fitting parameters.

Shift Factor Function

For fitting time-temperature shift factor functions following second order polynomial expression is used:

$$\log\left[a_T\right] = a\,T_i^2 + b\,T_i + c\,. \tag{3}$$

In Eq. (3), parameters *a*, *b*, and, *c* are fitting parameters.

Test Results

The results of |*E**| with δ testing, and hence development of the mastercurves and shift factor functions of the AC mixtures are presented in the following sub-sections.

Sample: SPIV PG70-22

Figures 1(a), 1(b), 1(c), and 1(d) show the average log-|*E**| versus log-frequency plot (also called isothermal curves), average |*E**| versus temperature plot (also called Isochronal curves), the Cole and Cole plane (or complex plane) plot, and the average *δ* versus average log-|*E**| plot (black space plot) at various test temperatures and frequencies for the SPIV PG70-22 AC sample.

Figure 2(a) shows the development of |E*|-mastercurve by horizontally shifting the tested |E*| at different temperatures and frequencies. The figure also shows the sigmoidal fitting of the |E*|-mastercurve by the expression given in Equation (1). The fitting statistics are also included in this figure showing the value of coefficient of determination (R^2) to be very close to unity. Figure 2(b) shows the tested, fitted, and after that smoothened |E*|-mastercurves for the SPIV PG70-22 AC sample. The 30 smoothened |E*| data points were evaluated for later use.

Figure 3(a) shows the development of δ-mastercurve for SPIV PG70-22 AC sample by horizontally shifting the tested δ at different temperatures and frequencies. The same temperature-frequency shift factors which were found while generating |E*|-mastercurve were used also for generating δ-mastercurve. The figure also shows the fitted δ-mastercurve by the expression given in Equation (2). The fitting statistics are also included in this figure. Figure 3(b) shows the tested, fitted, and smoothened δ-mastercurves for the SPIV PG70-22 AC mixture. The 30 smoothened δ-data points were evaluated for later use.

Figure 4 shows the temperature shift factors of SPIV PG70-22 AC mixture and the shift factor function fitted by the expression given in Equation (3).

Table 2 shows the summary of all the fitted parameters for the |E*| and δ-mastercurves, and the shift factor function.

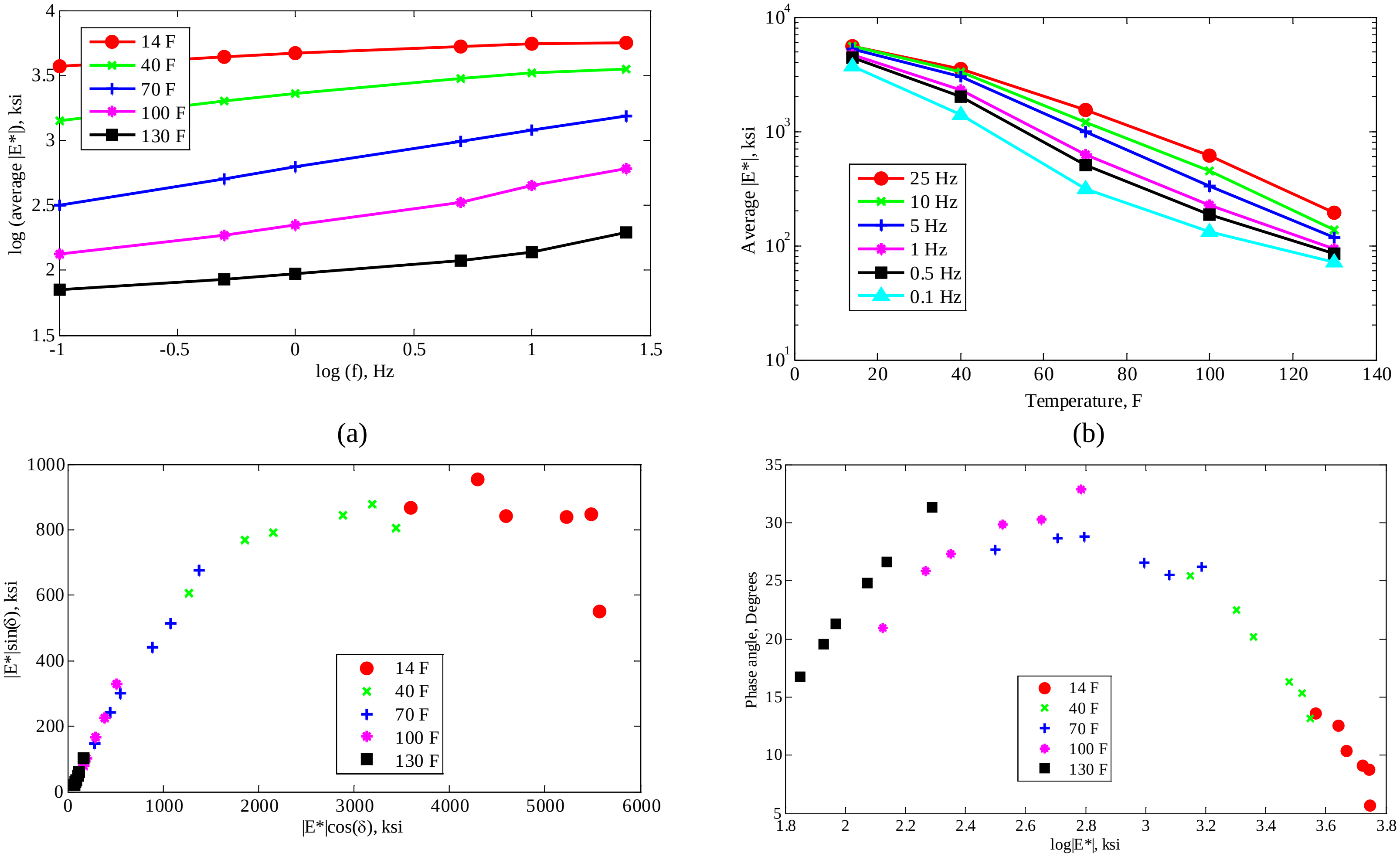

(a)

(b)

(c)

(d)

Figure 1 (a) Isothermal curves, (b) isochronal curves, (c) the complex plane plot, and (d) the black space plot for the SPIV PG70-22 AC mixture.

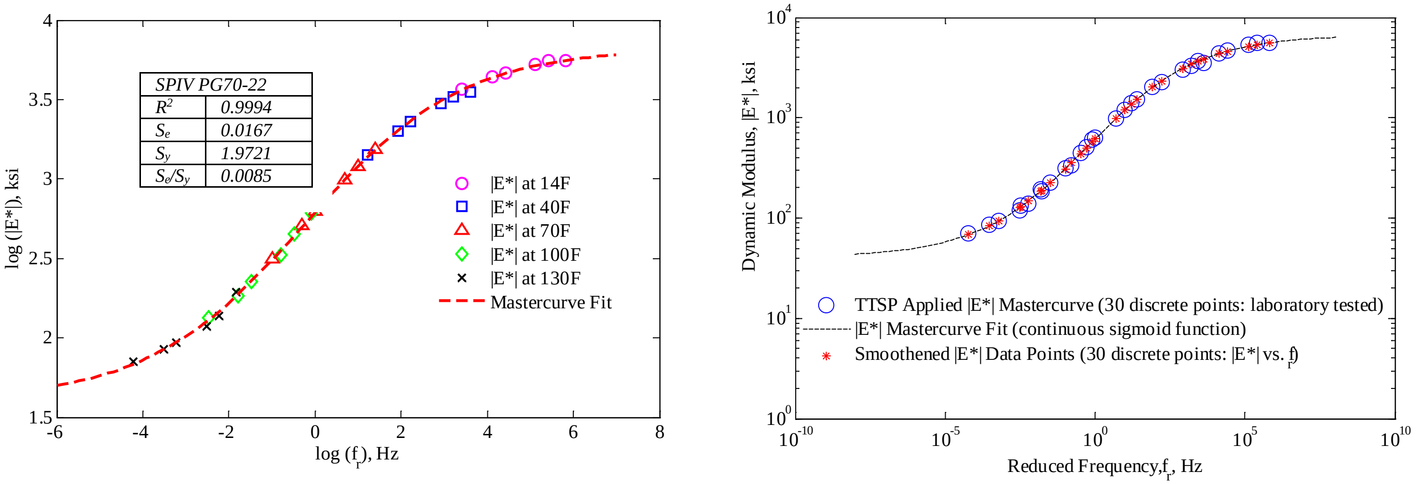

(a) (b)

Figure 2 (a) Development and fitting of log |E*|-mastercurve, (b) tested, fitted, and smoothened |E*|-mastercurve in log-log scale for SPIV PG70-22 AC mixture.

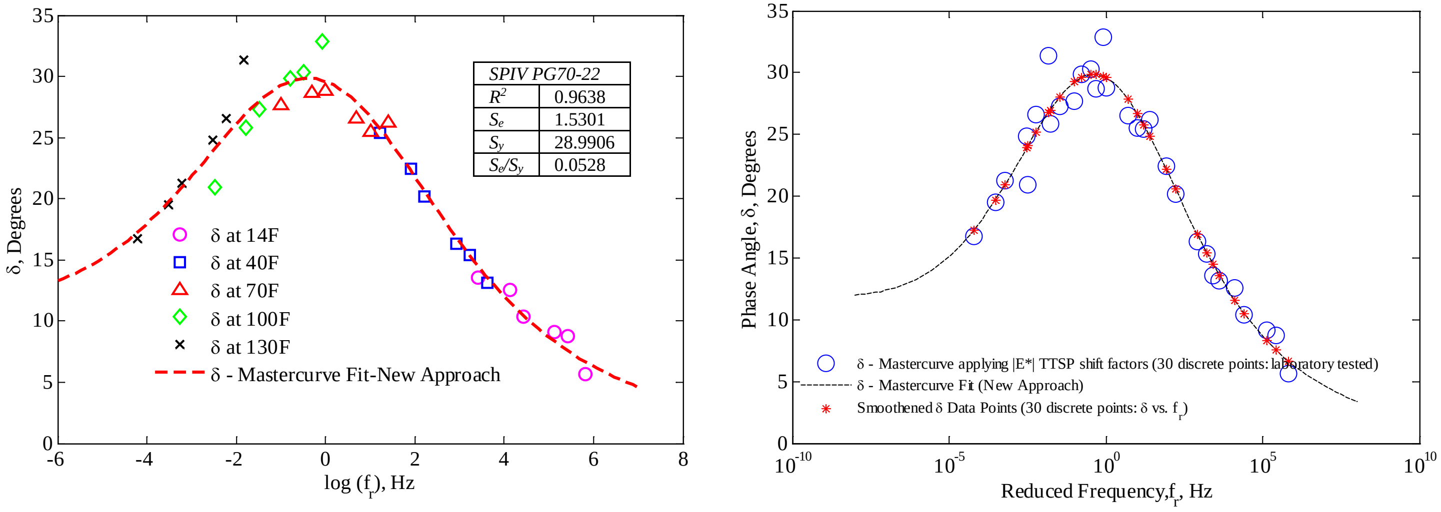

(a) (b)

Figure 3 (a) Fitting of δ-mastercurve, and (b) tested, fitted, and smoothened δ-mastercurve in semi-log scale for SPIV PG70-22 AC mixture.

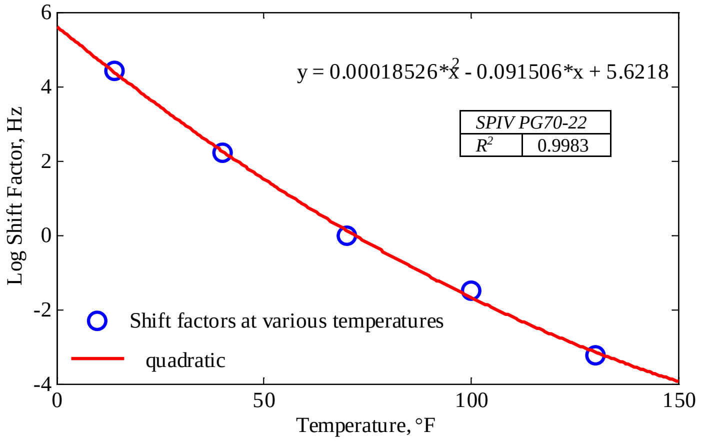

Figure 4 Temperature shift factor function for SPIV PG70-22 AC mixture.

Table 2. Summary of Fitted Parameters for SPIV PG70-22 AC Mixture

|E*|-Mastercurve Parameters ($T_{ref.}$ = 70 °F)	**α**	**β**	**δ**	**γ**
Values	2.2169	-0.1309	1.6082	-0.5466
δ-Mastercurve Parameters ($T_{ref.}$ = 70 °F)	**ξ_1**	**ξ_2**	**ξ_3**	
Values	0.1144	-0.0091	0.8487	
Shift Factor (a_T) Function Parameters	**a**	**b**	**c**	
Values	0.000185	-0.091506	5.6218	

Sample: SPIV PG76-22

Figures 5(a), 5(b), 5(c), and 5(d) show the average log-|*E**| versus log-frequency plot (also called isothermal curves), average |*E**| versus temperature plot (also called Isochronal curves), the Cole and Cole plane (or complex plane) plot, and the average δ versus average log-|*E**| plot (black space plot) at various test temperatures and frequencies for the SPIV PG76-22 AC sample.

Figure 6(a) shows the development of |*E**|-mastercurve by horizontally shifting the tested |*E**| at different temperatures and frequencies. The figure also shows the sigmoidal fitting of the |*E**|-mastercurve by the expression given in Equation (1). The fitting statistics are also included in this figure showing the value of coefficient of determination (R^2) to be very close to unity. Figure 6(b) shows the tested, fitted, and after that smoothened |*E**|-mastercurves for the SPIV PG76-22 AC sample. The 30 smoothened |*E**| data points were evaluated for later use.

Figure 7(a) shows the development of δ-mastercurve for SPIV PG76-22 AC sample by horizontally shifting the tested δ at different temperatures and frequencies. The same temperature-frequency shift factors which were found while generating |*E**|-mastercurve were used for generating δ-mastercurve. The figure also shows the fitted δ-mastercurve by the expression given in Equation (2). The fitting statistics are also included in this figure. Figure 3(b) shows the tested, fitted, and smoothened δ-mastercurves for the SPIV PG76-22 AC mixture. The 30 smoothened δ-data points were evaluated for later use.

Figure 8 shows the temperature shift factors of SPIV PG76-22 AC mixture and the shift factor function fitted by the expression given in Equation (3).

Table 3 shows the summary of all the fitted parameters for the $|E^*|$ and δ-mastercurves, and the shift factor function for the SPIV PG76-22 AC mixture.

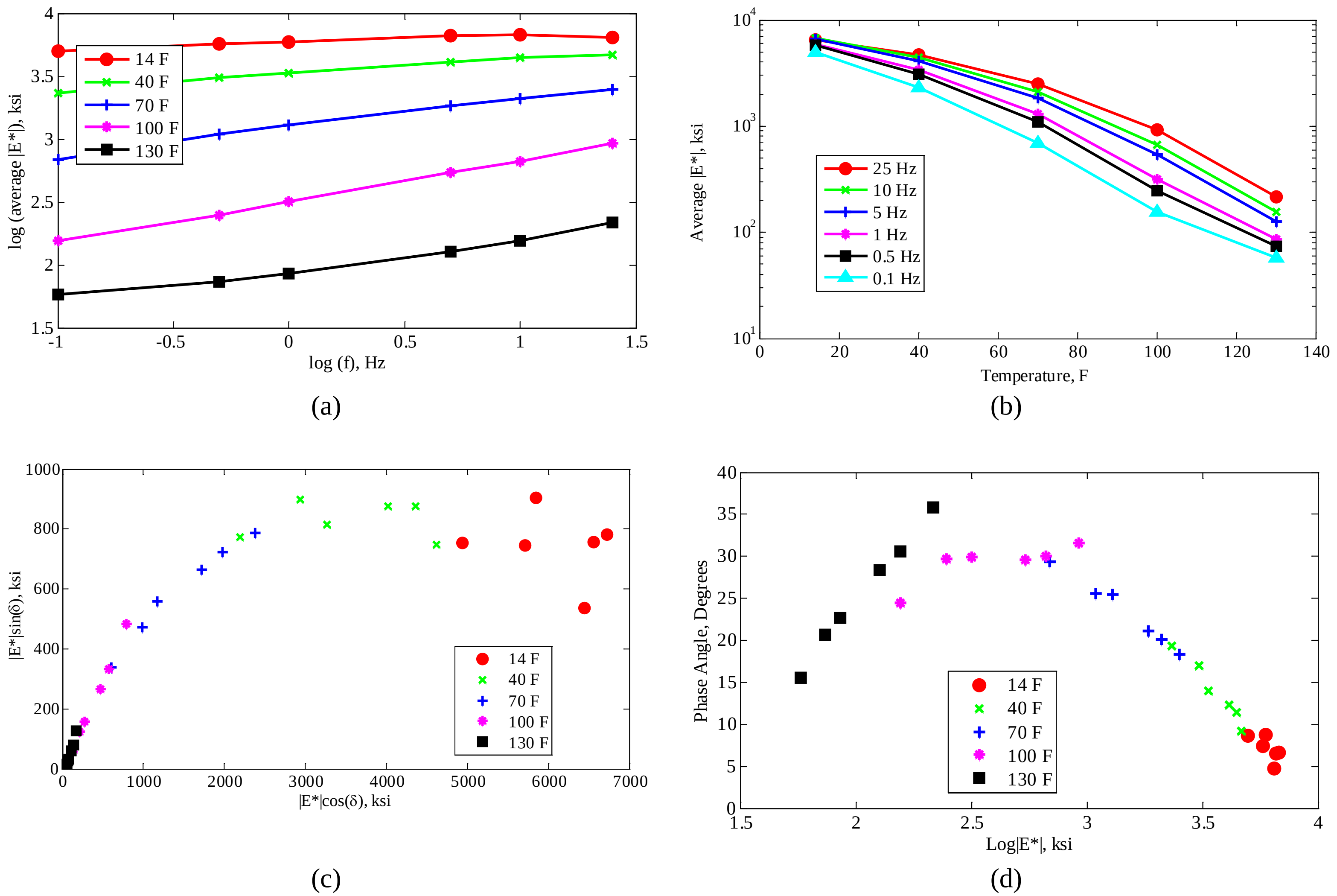

Figure 5 (a) Isothermal curves, (b) isochronal curves, (c) the complex plane plot, and (d) the black space plot for the SPIV PG76-22 AC mixture.

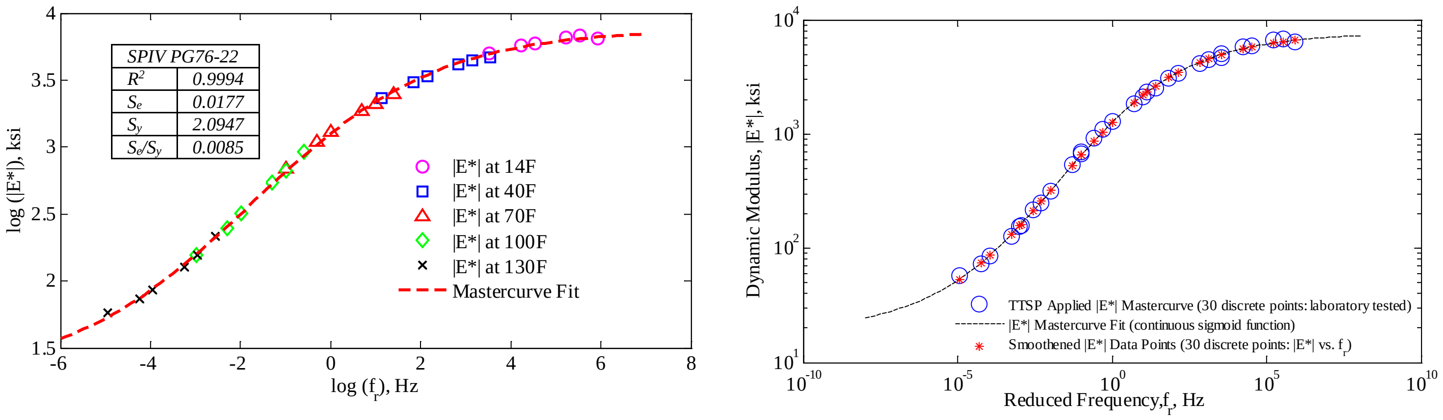

(a)

(b)

Figure 6 (a) Development and fitting of log |E*|-mastercurve, (b) tested, fitted, and smoothened |E*|-mastercurve in log-log scale for SPIV PG76-22 AC mixture.

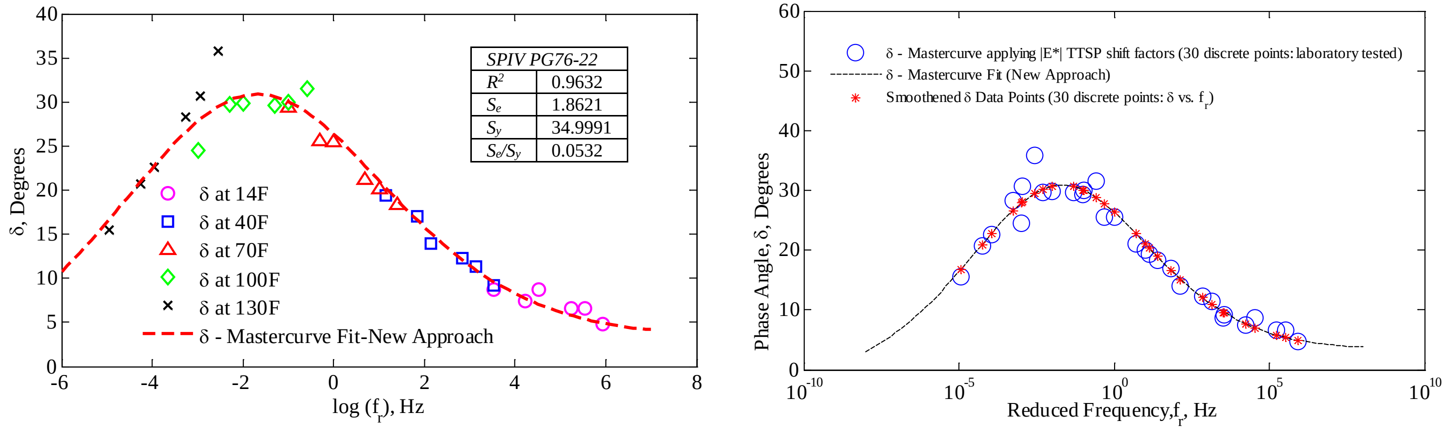

(a)

(b)

Figure 7 (a) Fitting of δ-mastercurve, and (b) tested, fitted, and smoothened δ-mastercurve in semi-log scale for SPIV PG76-22 AC mixture.

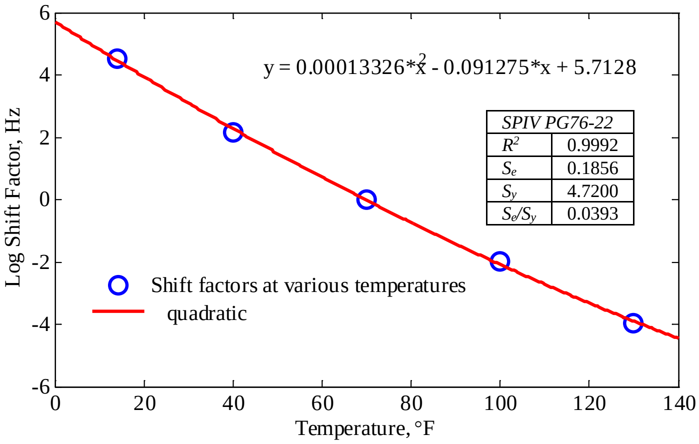

Figure 8 Temperature shift factor function for SPIV PG76-22 AC mixture.

Table 3. Summary of Fitted Parameters for SPIV PG76-22 AC Mixture

|E*|-Mastercurve Parameters ($T_{ref.}$ = 70 °F)	**α**	**β**	**δ**	**γ**
Values	2.6146	-0.8527	1.2688	-0.4837
δ-Mastercurve Parameters ($T_{ref.}$ = 70 °F)	**ξ_1**	**ξ_2**	**ξ_3**	
Values	0.0017	0.0058	1.1019	
Shift Factor (a_T) Function Parameters	**a**	**b**	**c**	
Values	0.000133	-0.091275	5.7128	

Sample: SPIII PG70-22

Figures 9(a), 9(b), 9(c), and 9(d) show the average log-|*E**| versus log-frequency plot (also called isothermal curves), average |*E**| versus temperature plot (also called Isochronal curves), the Cole and Cole plane (or complex plane) plot, and the average δ versus average log-|*E**| plot (black space plot) at various test temperatures and frequencies for the SPIII PG70-22 AC sample.

Figure 10(a) shows the development of |*E**|-mastercurve by horizontally shifting the tested |*E**| at different temperatures and frequencies. The figure also shows the sigmoidal fitting of the |*E**|-mastercurve by the expression given in Equation (1). The fitting statistics are also included in this figure showing the value of coefficient of determination (R^2) to be very close to unity. Figure 10(b) shows the tested, fitted, and after that smoothened |*E**|-mastercurves for the SPIII PG70-22 AC sample. The 30 smoothened |*E**| data points were evaluated for later use.

Figure 11(a) shows the development of δ-mastercurve for SPIII PG70-22 AC sample by horizontally shifting the tested δ at different temperatures and frequencies. The same temperature-frequency shift factors which were found while generating |*E**|-mastercurve were used for generating δ-mastercurve. The figure also shows the fitted δ-mastercurve by the expression given in Equation (2). The fitting statistics are also included in this figure. Figure 3(b) shows the tested, fitted, and smoothened δ-mastercurves for the SPIII PG70-22 AC mixture. The 30 smoothened δ-data points were evaluated for later use.

Figure 12 shows the temperature shift factors of SPIII PG70-22 AC mixture and the shift factor function fitted by the expression given in Equation (3).

Table 4 shows the summary of all the fitted parameters for the |*E**| and δ-mastercurves, and the shift factor function for the SPIII PG70-22 AC mixture.

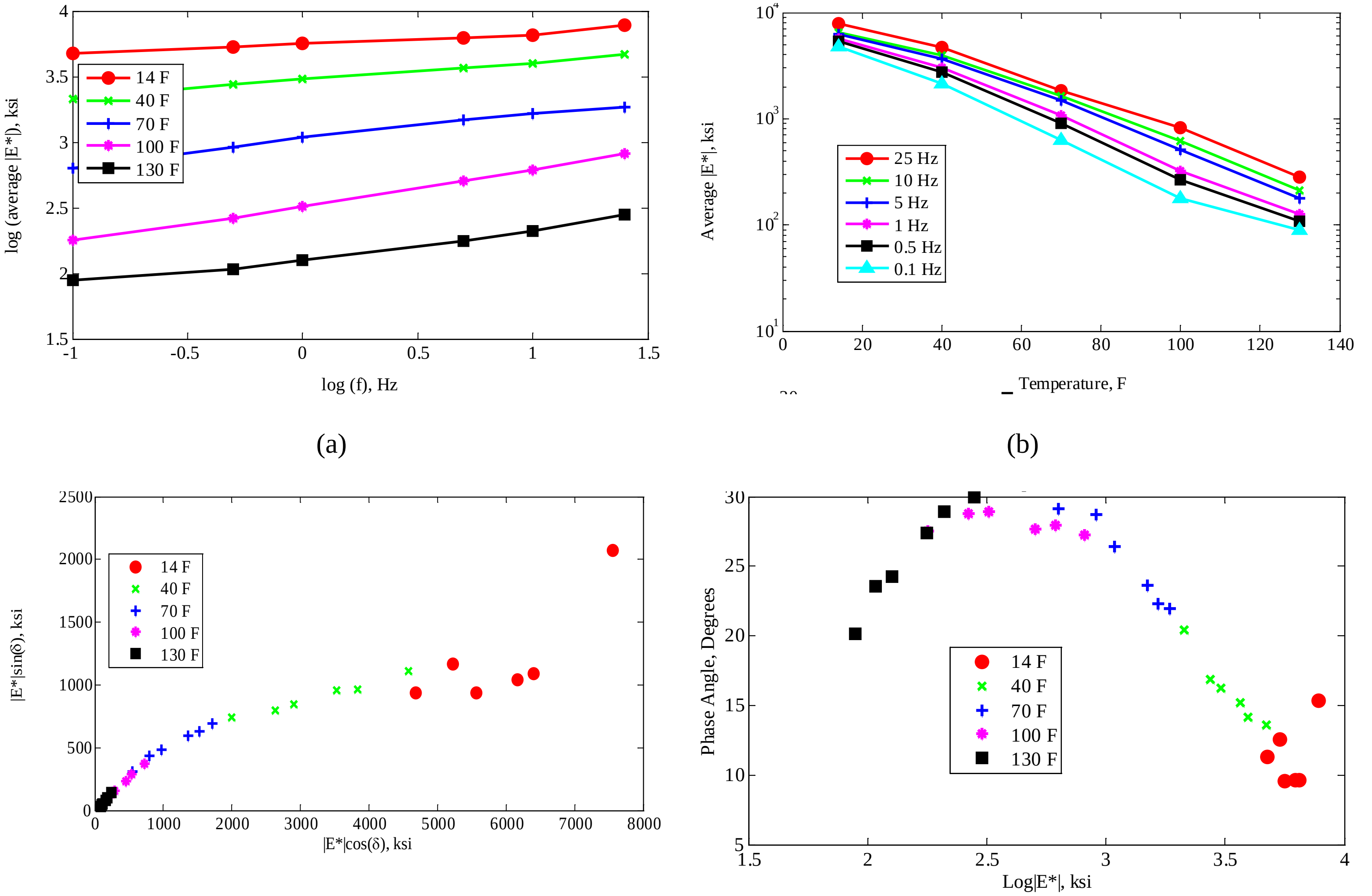

(a) (b)

(c) (d)

Figure 9 (a) Isothermal curves, (b) isochronal curves, (c) the complex plane plot, and (d) the black space plot for the SPIII PG70-22 AC mixture.

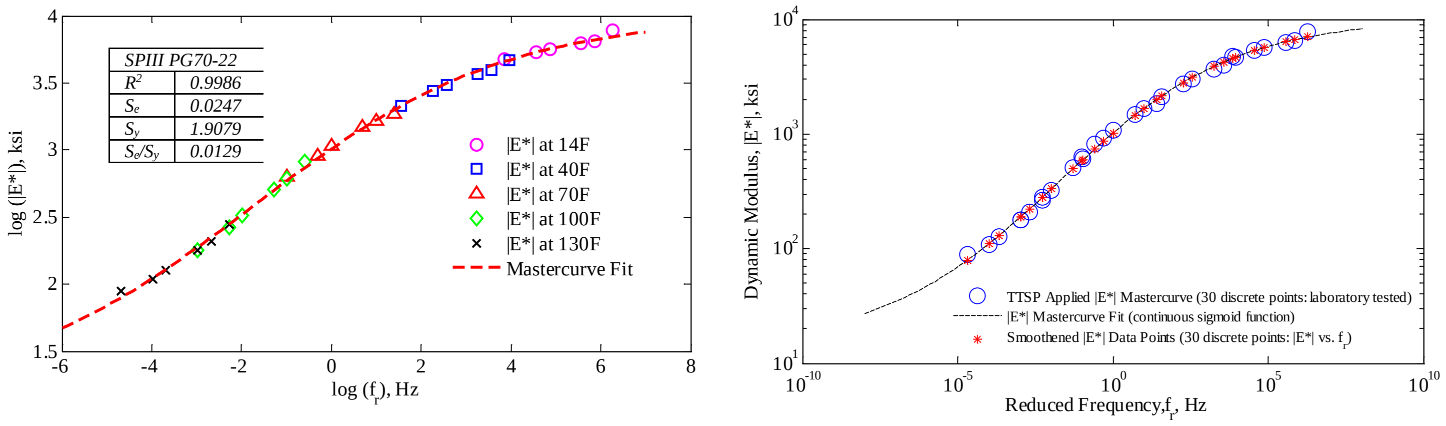

(a) (b)

Figure 10 (a) Development and fitting of log |E*|-mastercurve, (b) tested, fitted, and smoothened |E*|-mastercurve in log-log scale for SPIII PG70-22 AC mixture.

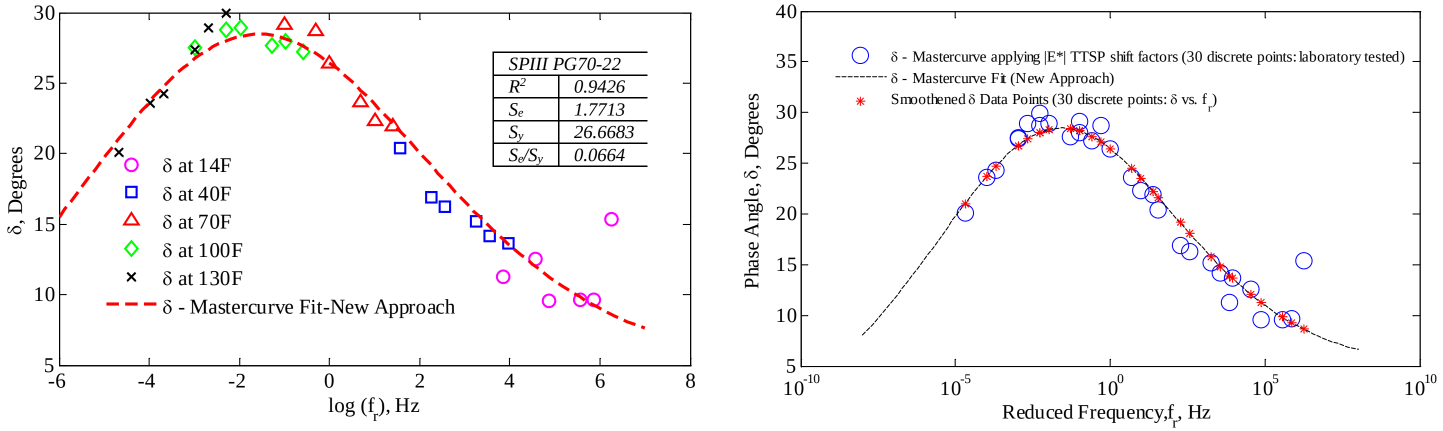

(a) (b)

Figure 11 (a) Fitting of δ-mastercurve, and (b) tested, fitted, and smoothened δ-mastercurve in semi-log scale for SPIII PG70-22 AC mixture.

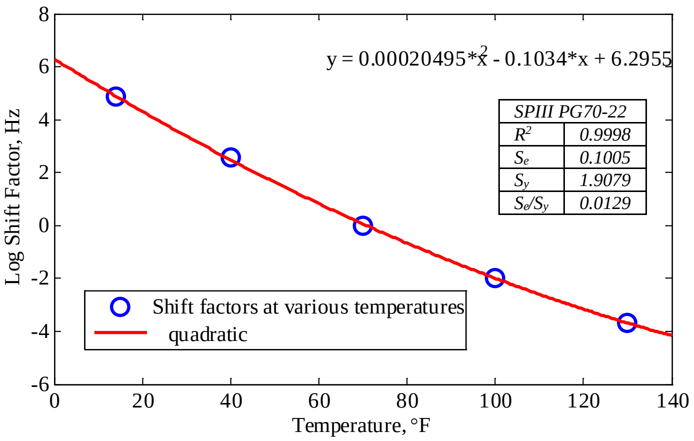

Figure 12 Temperature shift factor function for SPIII PG70-22 AC mixture.

Table 4. Summary of Fitted Parameters for SPIII PG70-22 AC Mixture

|E*|-Mastercurve Parameters ($T_{ref.}$ = 70 °F)	**α**	**β**	**δ**	**γ**
Values	2.8502	-0.6227	1.1529	-0.3540
δ-Mastercurve Parameters ($T_{ref.}$ = 70 °F)	**ξ_1**	**ξ_2**	**ξ_3**	
Values	0.0099	0.0058	1.2543	
Shift Factor (a_T) Function Parameters	**a**	**b**	**c**	
Values	0.000205	-0.1034	6.2955	

Sample: SPIII PG76-22

Figures 13(a), 13(b), 13(c), and 13(d) show the average log-|*E**| versus log-frequency plot (also called isothermal curves), average |*E**| versus temperature plot (also called Isochronal curves), the Cole and Cole plane (or complex plane) plot, and the average δ versus average log-|*E**| plot (black space plot) at various test temperatures and frequencies for the SPIII PG76-22 AC sample.

Figure 14(a) shows the development of |*E**|-mastercurve by horizontally shifting the tested |*E**| at different temperatures and frequencies. The figure also shows the sigmoidal fitting of the |*E**|-mastercurve by the expression given in Equation (1). The fitting statistics are also included in this figure showing the value of coefficient of determination (R^2) to be very close to unity. Figure 14(b) shows the tested, fitted, and after that smoothened |*E**|-mastercurves for the SPIII PG76-22 AC sample. The 30 smoothened |*E**| data points were evaluated for later use.

Figure 15(a) shows the development of δ-mastercurve for SPIII PG76-22 AC sample by horizontally shifting the tested δ at different temperatures and frequencies. The same temperature-frequency shift factors which were found while generating |*E**|-mastercurve were used for generating δ-mastercurve. The figure also shows the fitted δ-mastercurve by the expression given in Equation (2). The fitting statistics are also included in this figure. Figure 15(b) shows the tested, fitted, and smoothened δ-mastercurves for the SPIII PG76-22 AC mixture. The 30 smoothened δ-data points were evaluated for later use.

Figure 16 shows the temperature shift factors of SPIII PG76-22 AC mixture and the shift factor function fitted by the expression given in Equation (3).

Table 5 shows the summary of all the fitted parameters for the |*E**| and δ-mastercurves, and the shift factor function for the SPIII PG76-22 AC mixture.

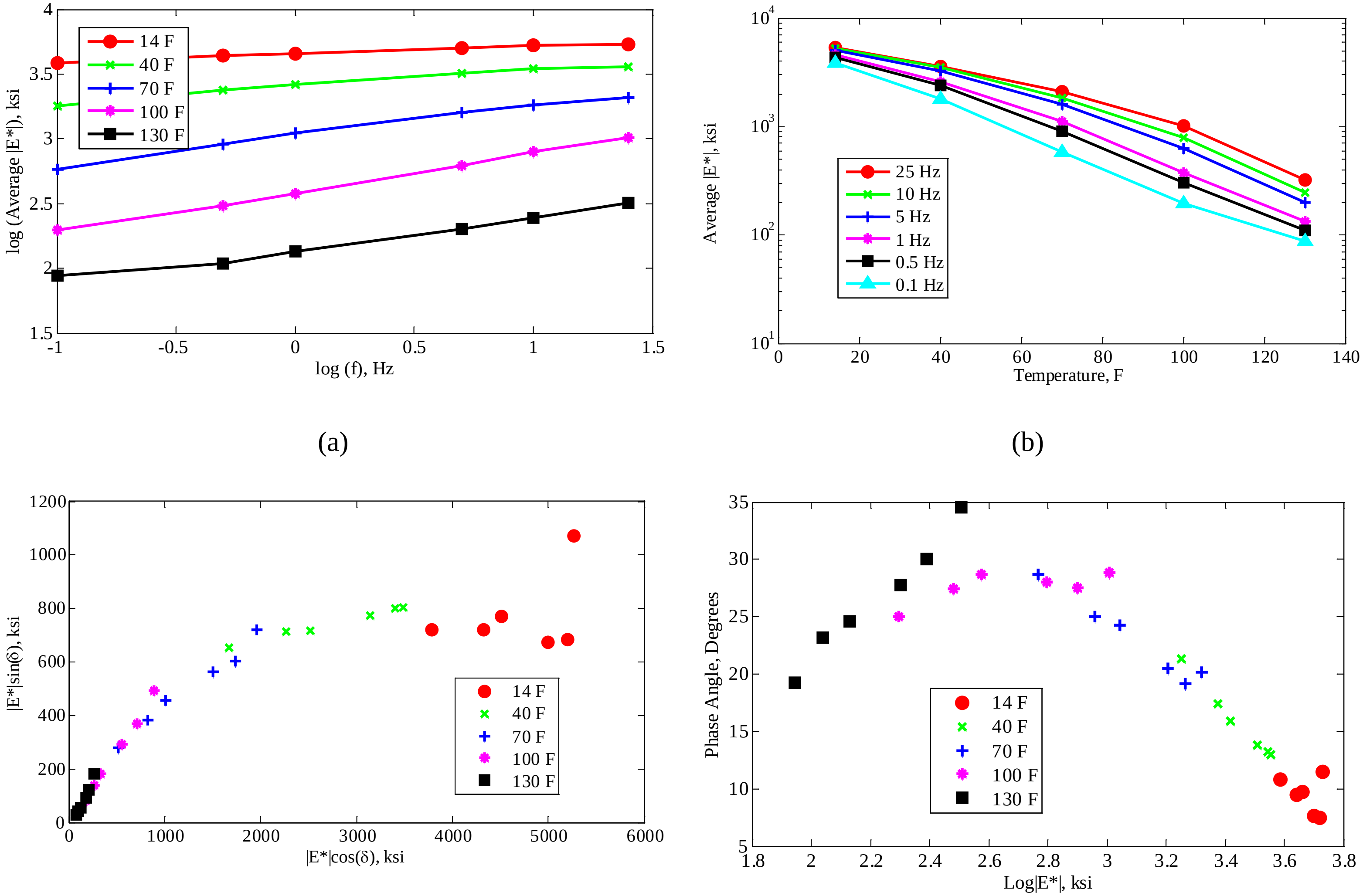

(a)

(b)

(c)

(d)

Figure 13 (a) Isothermal curves, (b) isochronal curves, (c) the complex plane plot, and (d) the black space plot for the SPIII PG76-22 AC mixture.

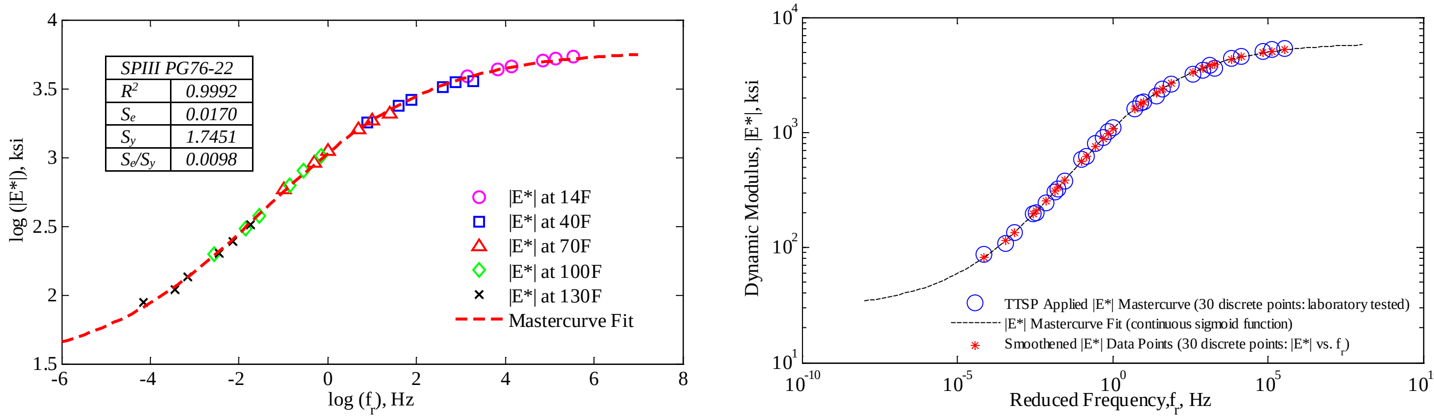

(a) (b)

Figure 14 (a) Development and fitting of log |E*|-mastercurve, (b) tested, fitted, and smoothened |E*|-mastercurve in log-log scale for SPIII PG76-22 AC mixture.

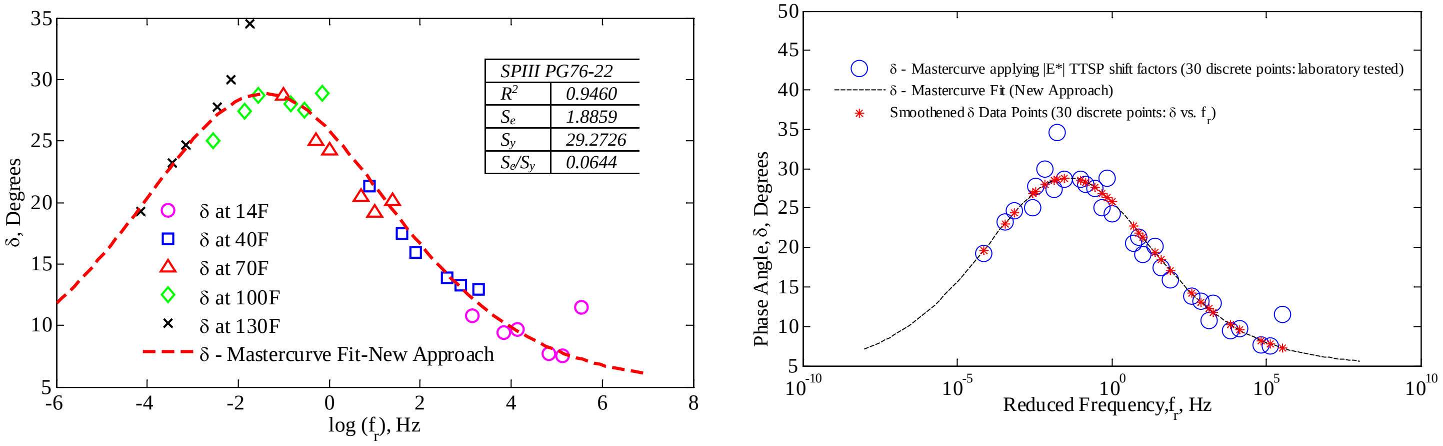

(a) (b)

Figure 15 (a) Fitting of δ-mastercurve, and (b) tested, fitted, and smoothened δ-mastercurve in semi-log scale for SPIII PG76-22 AC mixture.

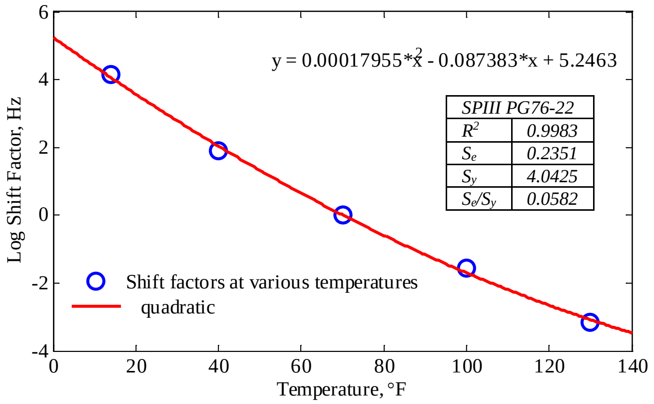

Figure 16 Temperature shift factor function for SPIII PG76-22 AC mixture.

Table 5. Summary of Fitted Parameters for SPIII PG76-22 AC Mixture

|E*|-Mastercurve Parameters ($T_{ref.}$ = 70 °F)	**α**	**β**	**δ**	**γ**
Values	2.3131	-0.7435	1.4634	-0.5216
δ-Mastercurve Parameters ($T_{ref.}$ = 70 °F)	**ξ_1**	**ξ_2**	**ξ_3**	
Values	0.0794	0.0008	0.8975	
Shift Factor (a_T) Function Parameters	**a**	**b**	**c**	
Values	0.000180	-0.087383	5.2463	

Task 3: Interconversion of Dynamic/Complex Modulus to Creep Compliance and Relaxation Modulus

The overview of the numerical interconversion method used in this study to convert one material function to another is given in the following paragraphs.

Numerical Method of Interconversion

The relaxation modulus $E(t)$ derived from the generalized Maxwell model (also called Wiechert model) consisting of m Maxwell elements connected in parallel is given by,

$$E(t) = E_e + \sum_{i=1}^{m} E_i e^{-(t/\rho_i)} \tag{4}$$

where E_e is the equilibrium modulus or long-time modulus; E_i are the relaxation strengths; and ρ_i are the relaxation times. The parameters, E_e, E_i, and ρ_i are positive constants. The Equation (4) is also known as Prony series representation of $E(t)$.

The creep compliance $D(t)$ can be represented by generalized Voigt model (or Kelvin model) which consists of a spring and a dashpot and n Voigt elements connected in series, and can be given as,

$$D(t) = D_g + \frac{1}{\eta_0} + \sum_{j=1}^{n} D_j (1 - e^{-(t/\tau_j)}) \tag{5}$$

where D_g is the glassy compliance; η_0 is the zero-shear or long-time viscosity; D_j are the retardation strengths; and τ_j are the retardation times; all are positive constants. The constants in Equations (4) and (5) can be obtained by fitting these expressions to the available experimental data. Note that, for viscoelastic solids like asphalt concrete, $\eta_0 \to \infty$; therefore, the second term in Equation (5) vanishes.

The well-known Boltzmann superposition integral representing stress-strain relation for a linear viscoelastic material can be given as:

$$\sigma(t) = \int_0^t E(t-\tau) \frac{d\varepsilon(t)}{d\tau}\, d\tau\,. \tag{6}$$

From Equation (6) the integral relationship between the uniaxial relaxation modulus $E(t)$ and creep compliance $D(t)$ can be found as:

$$\int_0^t E(t-\tau) \frac{dD(\tau)}{d\tau}\, d\tau = 1 \qquad (t > 0)\,. \tag{7}$$

Using relationship between Carson transforms of $E(t)$ and $D(t)$ (also called s-multiplied Laplace transform) and complex function E^*, and finally, Equation (4), the expressions for storage modulus $E'(\omega)$ and loss modulus $E''(\omega)$ can be given as:

$$E'(\omega) = E_e + \sum_{i=1}^{m} \frac{\omega^2 \rho_i{}^2 E_i}{\omega^2 \rho_i{}^2 + 1} \tag{8}$$

and,
$$E''(\omega) = \sum_{i=1}^{m} \frac{\omega \rho_i E_i}{\omega^2 \rho_i{}^2 + 1}\,. \tag{9}$$

The dynamic modulus $|E^*(\omega)|$ then can be found as:

$$\left|E^*(\omega)\right| = \sqrt{E'(\omega)^2 + E''(\omega)^2}\,. \tag{10}$$

and, the phase angle δ can be found as:

$$\delta = \tan^{-1}\left(\frac{E''(\omega)}{E'(\omega)}\right). \tag{11}$$

In Equations (8), (9), (10), and (11), ω is the angular frequency of loading; ρ_i and E_i ($i = 1, 2, \ldots, m$) can be found by fitting $E(t)$ to the Prony series expression of $E(t)$ given by Equation (4). The unknown retardation strengths, D_j ($j = 1, 2, \ldots, n$) and D_g can be found by using the Prony series coefficients of known $E(t)$ and thus solving the system of equations given as:

$$[\mathbf{A}]\{\mathbf{D}\} = \{\mathbf{B}\} \tag{12}$$

or, $A_{kj} D_j = B_k$ (summed on j; and k = 1, 2, …, p), where,

$$A_{kj} = \begin{cases} E_e(1 - e^{-(t_k/\tau_j)}) + \displaystyle\sum_{i=1}^{m} \frac{\rho_i\ E_i}{\rho_i - \tau_j}\left(e^{-(t_k/\rho_i)} - e^{-(t_k/\tau_j)}\right) & when \quad \rho_i \neq \tau_j \\ or & \\ E_e(1 - e^{-(t_k/\tau_j)}) + \displaystyle\sum_{i=1}^{m} \frac{t_k\ E_i}{\tau_j}\ e^{-(t_k/\rho_i)} & when \quad \rho_i = \tau_j \end{cases} \tag{13}$$

and,
$$\boldsymbol{B_k = 1 - \left(E_e + \sum_{i=1}^{m} E_i\ e^{-(t_k/\rho_i)}\right) \Big/ \left(E_e + \sum_{i=1}^{m} E_i\right)}. \tag{14}$$

The symbol, t_k denotes a discrete time. For the system of linear algebraic equation as in Equation (12), collocation method is effected when $p = n$ and the least squares method may be used when $p > n$. Equations (13) and (14) are found from substituting Equations (4) and (5) in Equation (7).

The retardation times, τ_j corresponding to a set of pre-selected relaxation times, ρ_i can be determined by a graphical root-finding method which uses the relationship between Carson transformed $E(t)$ and $D(t)$ given as:

$$\tilde{E}(s)\,\tilde{D}(s) = 1. \tag{15}$$

Here, $\tilde{E}(s) \equiv s\int_0^\infty E(t)\, e^{-st} dt$, and $\tilde{D}(s) \equiv s\int_0^\infty D(t)\, e^{-st} dt$, referred as operational modulus and operational compliance, respectively. When $E(t)$ and $D(t)$ are represented by the Equations (4) and (5), respectively, the operational modulus and compliance can be found as:

$$\tilde{E}(s) = E_e + \sum_{i=1}^{m} \frac{s\rho_i\, E_i}{s\rho_i + 1} \tag{16}$$

and,

$$\tilde{D}(s) = D_g + \frac{1}{\eta_0\, s} + \sum_{j=1}^{n} \frac{D_j}{s\tau_j + 1}. \tag{17}$$

Now, from Equation (16):

$$\lim_{s \to -(1/\rho_i)} \tilde{E}(s) = \pm\infty \qquad (i = 1, 2, ..., m) \tag{18}$$

Similarly, from Equation (17):

$$\lim_{s \to -(1/\tau_j)} \tilde{D}(s) = \pm\infty \qquad (j = 1, 2, ..., n) \tag{19}$$

From Equations (15) and (19), one can obtain:

$$\lim_{s \to -(1/\tau_j)} \tilde{E}(s) = 0 \qquad (j = 1, 2, ..., n) \tag{20}$$

The Equation (20) indicates that for given ρ_i and E_i, the τ_j can be determined by taking the negative reciprocal of the solutions of expression $\tilde{E}(s) = 0$ where $s < 0$. Graphical representation of the source function can be used to expedite the solution. Also, the relaxation and retardation times for viscoelastic solids are interlaced with each other as:

$$\rho_1 < \tau_1 < \rho_2 \quad \ldots \quad \rho_{N-1} < \tau_{N-1} < \rho_N < \tau_N \tag{21}$$

A typical graphical solution of the expression $\tilde{E}(s) = 0$ is presented in the Figure 17. This graphical solution was obtained while converting complex modulus E^* test data to $D(t)$ for asphalt concrete sample. Figure 17 shows $|\tilde{E}(s)|$ versus -1/s plot in logarithmic scale. The absolute value of $\tilde{E}(s)$ is used as because some of the negative numbers cannot be plotted in logarithmic scale. A total of 10,000 equidistant points in log-scale are plotted for the value of -1/s in between $1.0\text{x}10^{-8}$ to $1.0\text{x}10^{8}$. The abscissa corresponding to each maximum gives the known relaxation time, ρ_i, and the abscissa corresponding to each minimum gives the unknown retardation time, τ_j.

To evaluate $E(t)$ from $D(t)$ one need to fit the creep compliance data to Prony series representation of $D(t)$ given in Equation (5). This fitting operation will ultimately evaluate the values of D_j, τ_j, and D_g. The unknown relaxation strengths, E_i ($i = 1, 2, \ldots, m$) and equilibrium modulus E_e then can be found by using the Prony series coefficients of known $D(t)$ and thus solving a system of equations similar to Equation (12) as:

$$[\mathbf{C}]\{\mathbf{E}\} = \{\mathbf{F}\} \tag{22}$$

or, $C_{ki}E_i = F_k$(summed on i; and k = 1, 2, …, p), where,

$$C_{ki} = \begin{cases} D_g e^{-(t_k/\rho_i)}) + \sum_{j=1}^{n} \frac{\rho_i D_j}{\rho_i - \tau_j}\left(e^{-(t_k/\rho_i)} - e^{-(t_k/\tau_j)}\right) & when \rho_i \neq \tau_j \\ \qquad\qquad or & \\ D_g e^{-(t_k/\rho_i)}) + \sum_{j=1}^{n} \frac{t_k D_j}{\tau_j} e^{-(t_k/\rho_i)} & when \rho_i = \tau_j \end{cases} \tag{23}$$

and,
$$F_k = 1 - \left(D_g + \sum_{j=1}^{n} D_j\left(1 - e^{-(t_k/\tau_j)}\right)\right) \Big/ \left(D_g + \sum_{j=1}^{n} D_j\right). \tag{24}$$

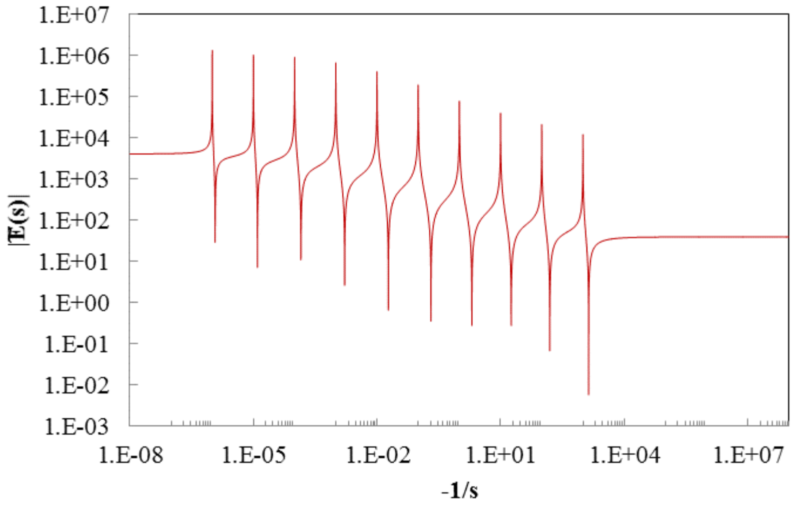

Figure 17 $\tilde{E}(s)$ **versus -1/s plot, a root finding by graphical method.**

Equations (23) and (24) also found from substituting Equations (4) and (5) in Equation (7). The relaxation times ρ_i corresponding to a set of selected retardation times τ_j can be determined by root-finding method using the relationship between Carson transformed $E(t)$ and $D(t)$.

From Equations (15) and (18), one can obtain:

$$\lim_{s \to -(1/\rho_i)} \tilde{D}(s) = 0 \qquad (i = 1, 2, \ldots, m)\,. \tag{25}$$

This also indicates, for given τ_j and D_j, the ρ_i can be determined by taking the negative reciprocal of the solutions of expression $\tilde{D}(s) = 0$ where $s < 0$. Similar graphical root finding method given in Figure 17 then can be used to evaluate the unknown ρ_i. After evaluating all the ρ_i, E_i and E_e, Equation 4 can be used to determine $E(t)$. Storage and loss modulus can be calculated by substituting Prony coefficients already determined in earlier section in the Equations (8) and (9), and finally the dynamic modulus and phase angle can be found by Equations (10) and (11), respectively.

Relaxation Modulus from Complex Modulus

Equation (8) can be used to fit storage modulus data which can be found from dynamic modulus or complex modulus test. This fitting operation will evaluate the Prony coefficients ρ_i, E_i, and E_e. To determine $E(t)$ Equation (4) can be used.

Creep Compliance from Complex Modulus

For $D(t)$, Equations (12) can be used to determine D_j. The same root finding method described in earlier sections can be employed to find the corresponding τ_j for the pre-selected ρ_i.

If the tested dynamic modulus values are found as a function of ordinary frequency (Hz), one must need to transform the ordinary frequency domain to angular frequency (rad/sec) to use this method of interconversion. It should be noted that for a given test data D_g and E_e can be determined from the following expressions:

$$D_g = \frac{1}{E_e + \sum_{i=1}^{m} E_i} \qquad \text{and,} \qquad E_e = \frac{1}{D_g + \sum_{j=1}^{n} D_j}. \tag{26}$$

Methodology Flow Chart

The overall methodology to convert E^* to E(t) and D(t) can be shown by Figure 18 below.

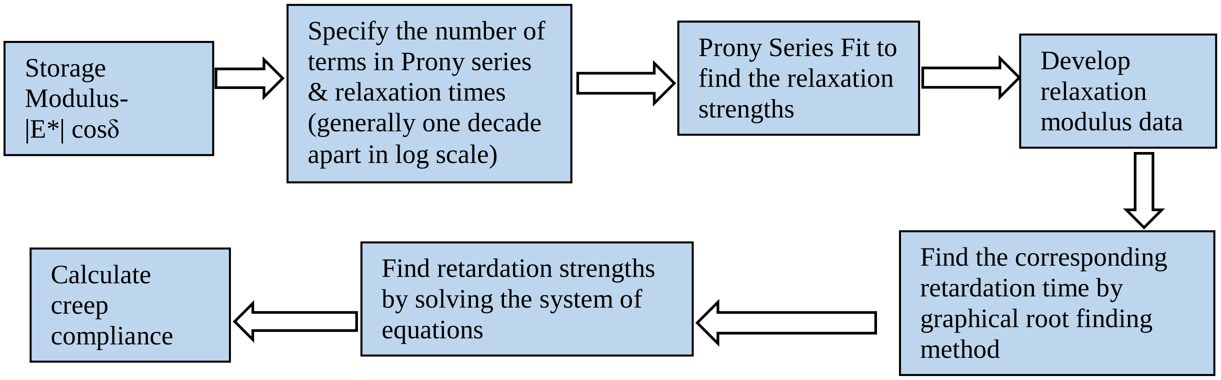

Figure 18 Methodology Flow Chart for converting *E data to *E*(*t*) and *D*(*t*).**

Results

The smoothened |E*| and δ data evaluated earlier were used to derive storage modulus of the modulus. The storage moduli were found by the following expression:

$$E(\omega)' = |E^*| \cos \delta \tag{27}$$

Table 6 summarizes the Prony series coefficients found for all four study mixtures.

The results (graphical) of interconversion of *E** to *D*(*t*) and *E*(*t*) for the study mixes are shown in the following sub-sections.

Table 6. Summary of Prony Series Coefficients for the Relaxation Modulus and Creep Compliance Functions

SPIV PG70-22		***SPIV PG76-22***		***SPIII PG70-22***		***SPIII PG76-22***	
ρ_i	E_i	ρ_i	E_i	ρ_i	E_i	ρ_i	E_i
2.000E-07	6.205E+02	4.000E-07	4.991E+02	3.000E-07	1.021E+03	5.000E-07	4.003E+02
2.000E-06	7.774E+02	4.000E-06	7.172E+02	3.000E-06	1.125E+03	5.000E-06	5.574E+02
2.000E-05	1.007E+03	4.000E-05	1.024E+03	3.000E-05	1.108E+03	5.000E-05	7.685E+02
2.000E-04	1.205E+03	4.000E-04	1.182E+03	3.000E-04	1.096E+03	5.000E-04	9.890E+02
2.000E-03	9.845E+02	4.000E-03	1.152E+03	3.000E-03	9.420E+02	5.000E-03	9.441E+02
2.000E-02	6.670E+02	4.000E-02	9.884E+02	3.000E-02	7.094E+02	5.000E-02	7.851E+02
2.000E-01	3.367E+02	4.000E-01	5.611E+02	3.000E-01	4.081E+02	5.000E-01	4.398E+02
2.000E+00	1.560E+02	4.000E+00	3.112E+02	3.000E+00	2.645E+02	5.000E+00	2.429E+02
2.000E+01	6.491E+01	4.000E+01	1.249E+02	3.000E+01	1.244E+02	5.000E+01	1.085E+02
2.000E+02	3.424E+01	4.000E+02	6.291E+01	3.000E+02	7.459E+01	5.000E+02	4.329E+01
2.000E+03	1.635E+01	4.000E+03	2.859E+01	3.000E+03	3.848E+01	5.000E+03	3.614E+01
E_e = 5.907E+01		E_e = 4.938E+01		E_e = 6.890E+01		E_e = 4.498E+01	
τ_j	D_j	τ_j	D_j	τ_j	D_j	τ_j	D_j
2.225E-07	1.889E-05	4.319E-07	1.163E-05	3.501E-07	2.324E-05	5.407E-07	1.462E-05
2.335E-06	3.095E-05	4.515E-06	2.032E-05	3.687E-06	3.747E-05	5.632E-06	2.464E-05
2.551E-05	5.837E-05	4.897E-05	3.957E-05	3.869E-05	5.832E-05	6.020E-05	4.534E-05
2.990E-04	1.316E-04	5.391E-04	7.463E-05	4.212E-04	1.036E-04	6.800E-04	9.448E-05
3.415E-03	2.756E-04	6.067E-03	1.465E-04	4.619E-03	1.921E-04	7.652E-03	1.863E-04
3.929E-02	6.319E-04	7.296E-02	3.472E-04	5.122E-02	3.857E-04	9.101E-02	4.323E-04
4.032E-01	1.335E-03	7.769E-01	7.226E-04	5.124E-01	6.605E-04	9.515E-01	8.706E-04
3.859E+00	2.543E-03	8.616E+00	1.721E-03	5.578E+00	1.362E-03	1.017E+01	1.905E-03
3.246E+01	3.429E-03	7.688E+01	3.089E-03	5.088E+01	2.107E-03	9.554E+01	3.572E-03
2.950E+02	4.273E-03	7.357E+02	5.483E-03	5.108E+02	3.637E-03	7.775E+02	4.196E-03
2.584E+03	4.032E-03	6.588E+03	8.445E-03	4.835E+03	5.803E-03	9.315E+03	1.070E-02
D_g = 1.687E-04		D_g = 1.492E-04		D_g = 1.433E-04		D_g = 1.866E-04	

Sample: SPIV PG70-22

Figure 19(a) shows the $E(\omega)$' function fitted by the Prony series representation of $E(\omega)$' given in Equation (8). The pre-defined relation times (ρ_i) and the coefficients E_i and E_e found by this fitting operation are summarized in Table 6. Once the coefficients are found the relaxation modulus as a function of time can be found by the expression given in Equation (4), which is shown in Figure 19(b). Figure 19(c) shows the operational modulus versus -1/s plot for determining retardation times (τ_i) corresponding to the pre-defined ρ_i. D_j and D_g are found by solving the system of equation given in Equation (12). These computed coefficients are also summarized in Table 6. Thus, Equation (5) was used the evaluated the creep compliance as a function of time which is shown in Figure 19(d).

Sample: SPIV PG76-22

Figure 20(a) shows the $E(\omega)$' function fitted by the Prony series representation of $E(\omega)$' given in Equation (8). The relaxation modulus as a function of time is shown in Figure 20(b). Figure 20(c) shows the operational modulus versus -1/s plot for determining retardation times (τ_i) corresponding to the pre-defined ρ_i. The creep compliance as a function of time is shown in Figure 20(d).

Sample: SPIII PG70-22

Figure 21(a) shows the $E(\omega)$' function fitted by the Prony series representation of $E(\omega)$' given in Equation (8). The relaxation modulus as a function of time is shown in Figure 21(b). Figure 21(c) shows the operational modulus versus -1/s plot for determining retardation times (τ_i) corresponding to the pre-defined ρ_i. The creep compliance as a function of time is shown in Figure 21(d).

Sample: SPIII PG76-22

Figure 22(a) shows the $E(\omega)$' function fitted by the Prony series representation of $E(\omega)$' given in Equation (8). The relaxation modulus as a function of time is shown in Figure 22(b). Figure 22(c) shows the operational modulus versus -1/s plot for determining retardation times (τ_i) corresponding to the pre-defined ρ_i. The creep compliance as a function of time is shown in Figure 22(d).

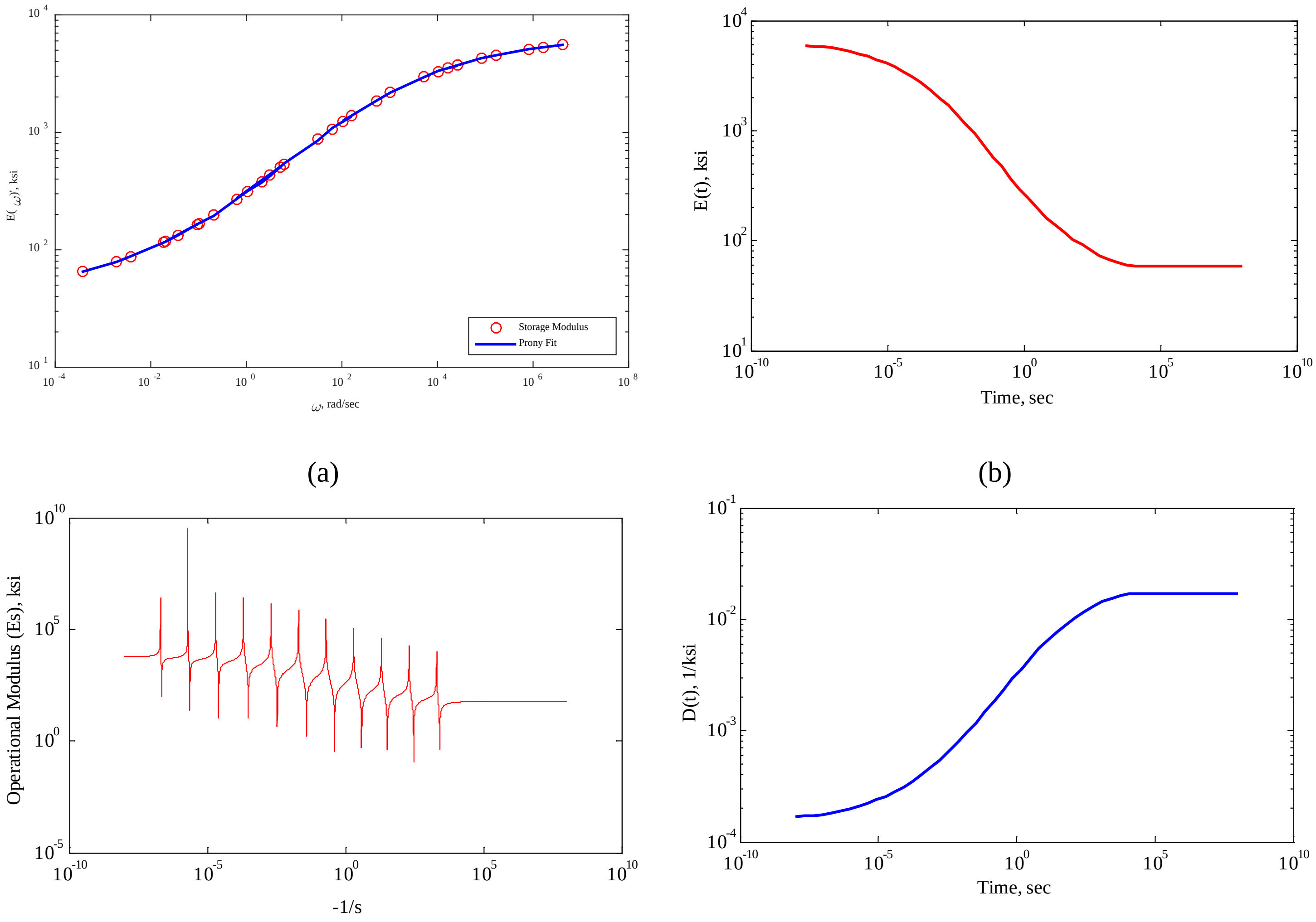

(a) (b)

(c) (d)

Figure 19 (a) Prony series fitting of the storage modulus, (b) converted relaxation modulus as a function of time, (c) evaluation of retardation times, and (d) converted creep compliance as a function of time for SPIV PG70-22 AC mixture.

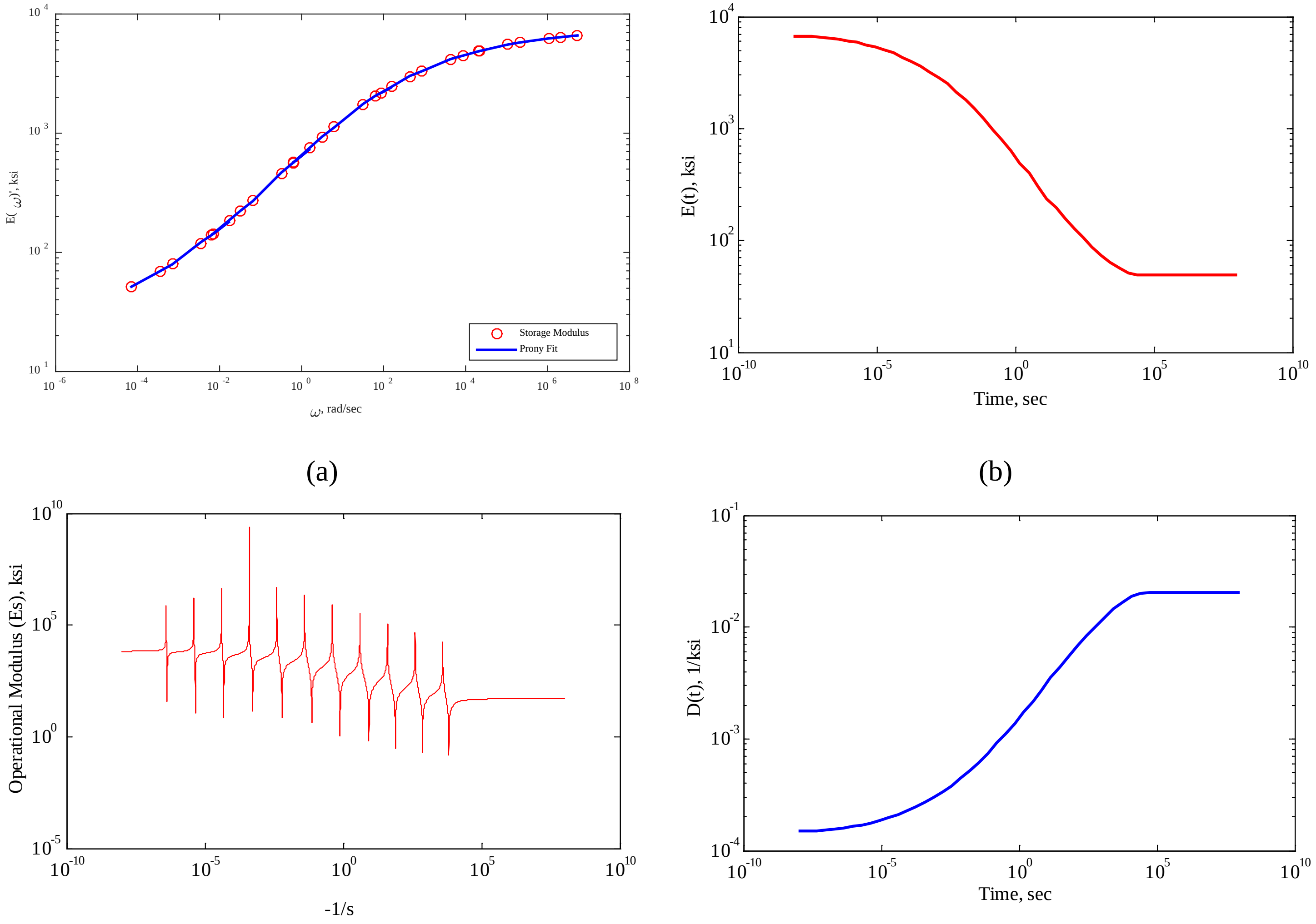

(a)

(b)

(c)

(d)

Figure 20 (a) Prony series fitting of the storage modulus, (b) converted relaxation modulus as a function of time, (c) evaluation of retardation times, and (d) converted creep compliance as a function of time for SPIV PG76-22 AC mixture.

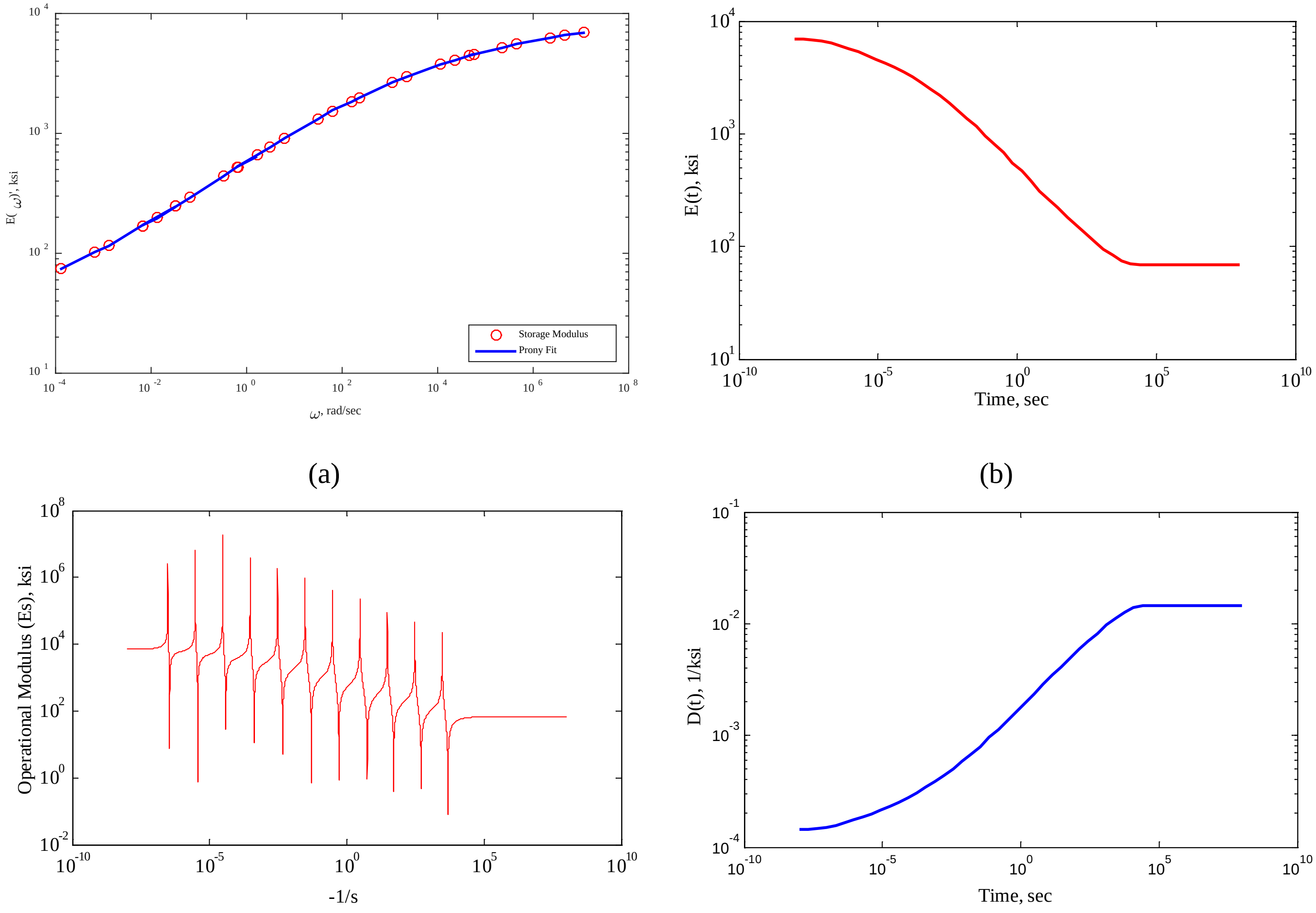

(a)

(b)

(c)

(d)

Figure 21 (a) Prony series fitting of the storage modulus, (b) converted relaxation modulus as a function of time, (c) evaluation of retardation times, and (d) converted creep compliance as a function of time for SPIII PG70-22 AC mixture.

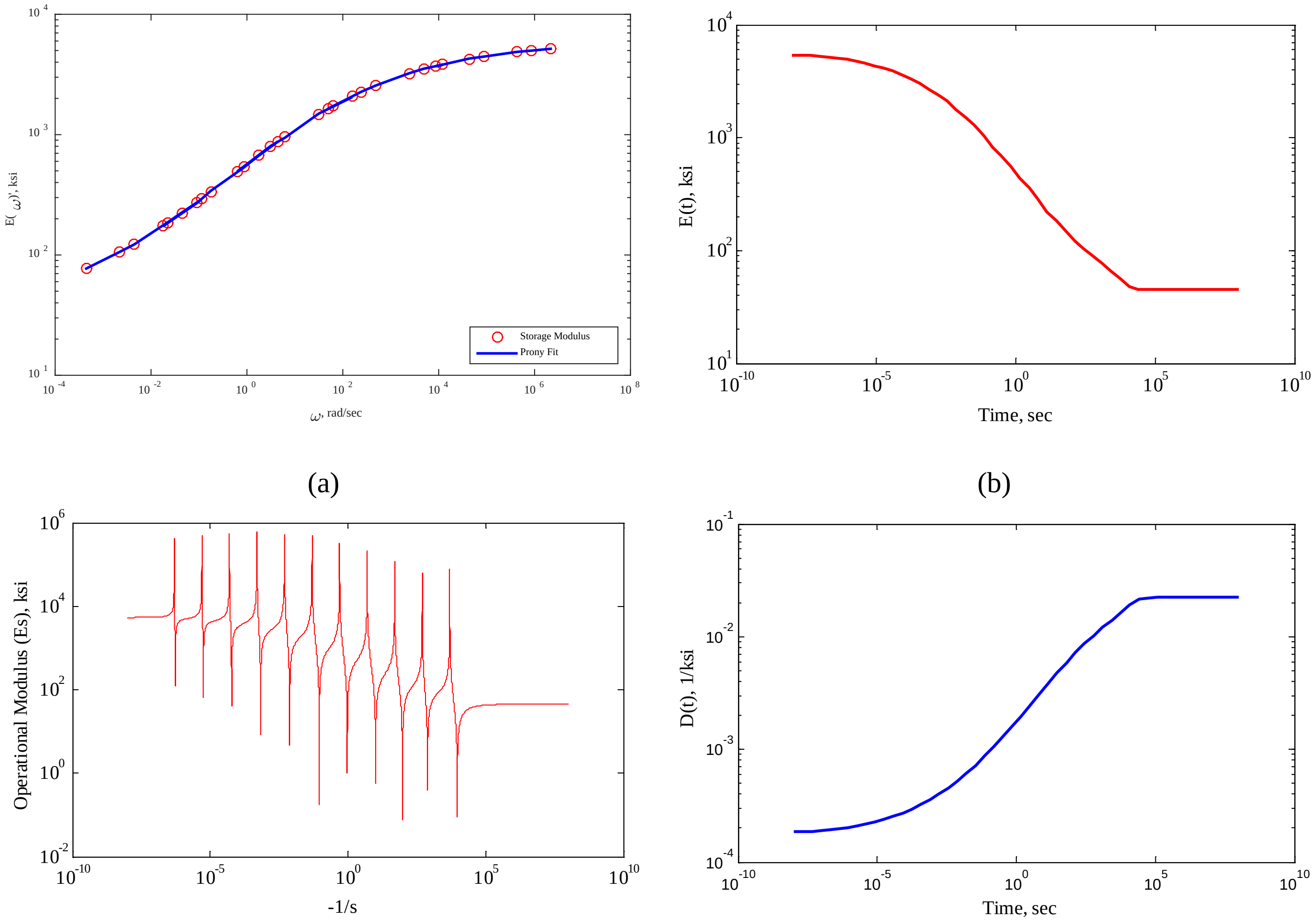
(a) (b) (c) (d)

Figure 22 (a) Prony series fitting of the storage modulus, (b) converted relaxation modulus as a function of time, (c) evaluation of retardation times, and (d) converted creep compliance as a function of time for SPIII PG76-22 AC mixture.

Task 4: Creep Compliance Testing and Validation of Interconversion

Uniaxial Creep Compliance Test

Creep tests were conducted for 1000 seconds on each of the specimens at five different temperatures, 14 °F, 40 °F, 70 °F, 100 °F, and 130 °F, starting at the lowest temperature and proceeding to the highest temperature. The applied stresses at each temperature level were approximated by trial to limit the total strain within 200 $\mu\varepsilon$ after 1000 seconds of test period. The creep compliance $D(t)$ was found by dividing the average creep strain of the two specimens by the input stress. The time temperature superposition principle was applied to develop average creep compliance mastercurve at 70 °F reference temperature. To have a smoother representation of creep compliance, the developed mastercurve was smoothened using piecewise-polynomial fit.

Results

Creep compliance test results and comparison to the interconverted creep compliances of all the AC mixtures considered in this study are presented in the following sections.

Sample: SPIV PG70-22

Development of Creep Compliance Function

Figure 23 shows a typical uniaxial (compressive) creep test performed on a specimen of the AC mixture SPIV PG70-22 at a temperature of 14 °F. The figure shows the applied constant stress and the associated creep strain over 1000 seconds time period. Figure 24 shows the creep compliance as a function of time at different temperatures and the developed mastercurve by horizontally shifting the creep compliance data (known also as the application of time-temperature superposition principal). Figure 25 shows the unsmooth and smoothened creep compliance function.

Comparison of Tested and Converted Creep Compliance Functions for SPIV PG70-22 AC Mixture

Figures 26(a) and 26(b) show the creep compliance functions obtained from laboratory test and converted from E^* test data in log-log and normal scales, respectively. Observing the creep compliance functions found from two different source, it can be said that the numerical method of interconversion discussed earlier gives a good estimation of creep compliance considering the specimen to specimen variation as well as the limitation associated with laboratory testing. The difference in these two compliance functions is more toward the higher reduced time region.

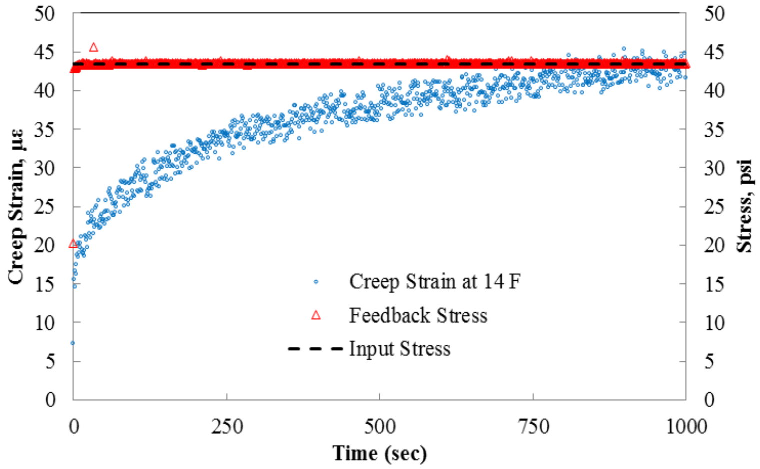

Figure 23 Typical uniaxial creep test.

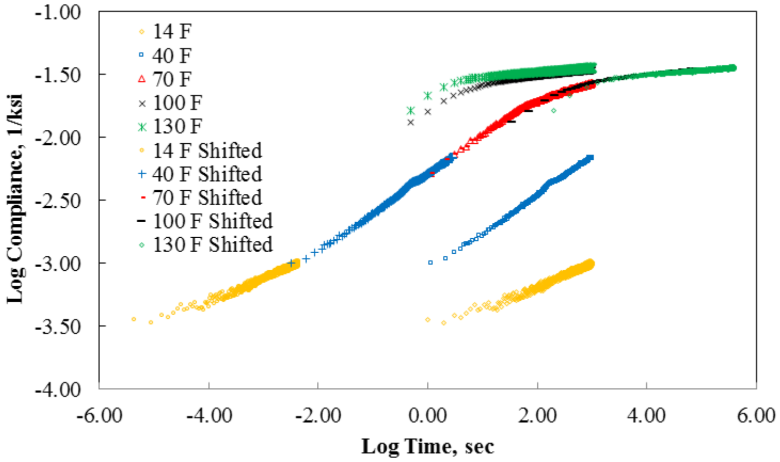

Figure 24 Development of creep compliance mastercurve.

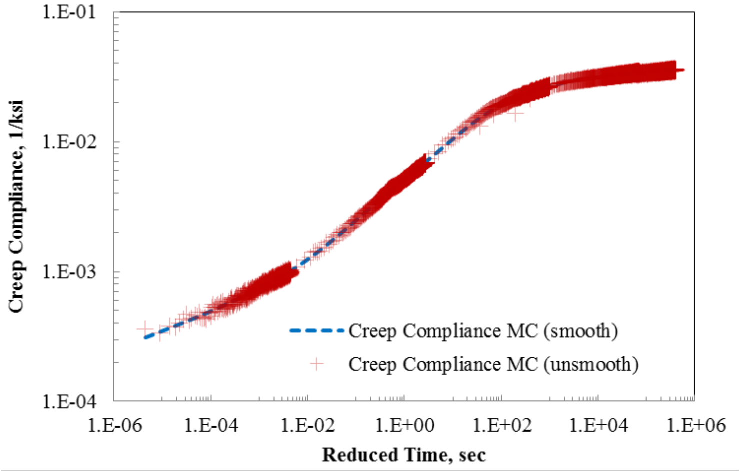

Figure 25 Unsmooth and smoothened creep compliance mastercurve.

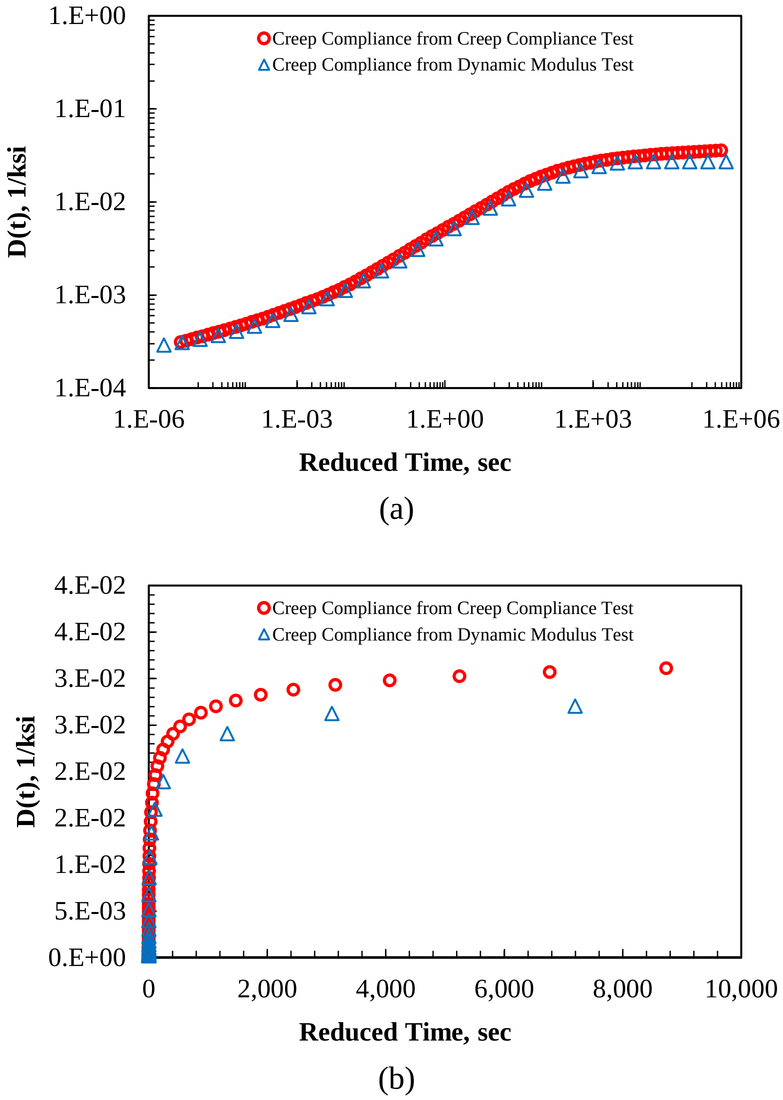

Figure 26 Laboratory tested and converted creep compliance functions: (a) in log-log scale, and (b) in normal scale (up to 10000 seconds reduced time).

Sample: SPIV PG76-22

Development of Creep Compliance Function

Figure 27 shows a typical uniaxial (compressive) creep test performed on a specimen of the AC mixture SPIV PG76-22 at a temperature of 14 °F. Similar as in previous, the figure shows the applied constant stress and the associated creep strain over 1000 seconds time period. Figure 28 shows the creep compliance as a function of time at different temperatures and the developed mastercurve by horizontally shifting the creep compliance data. Figure 29 shows the unsmooth and smoothened creep compliance function.

Comparison of Tested and Converted Creep Compliance Functions for SPIV PG76-22 AC Mixture

Figures 30(a) and 30(b) show the creep compliance functions obtained from laboratory test and converted from *E** test data in log-log and normal scales, respectively. Observing the creep compliance functions found from two different source, it can be said that the numerical method of interconversion discussed earlier gives a good estimation of creep compliance considering the specimen to specimen variation as well as the limitation associated with laboratory testing. The difference in these two compliance functions is more toward the higher reduced time region.

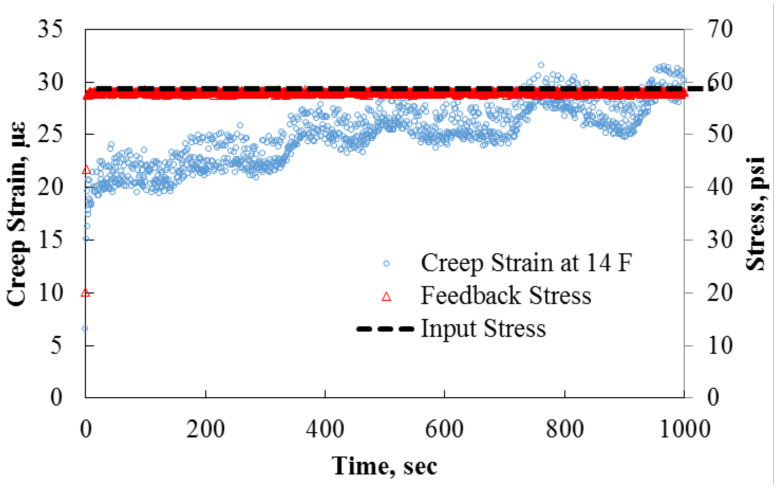

Figure 27 Typical uniaxial creep test at 14 °F.

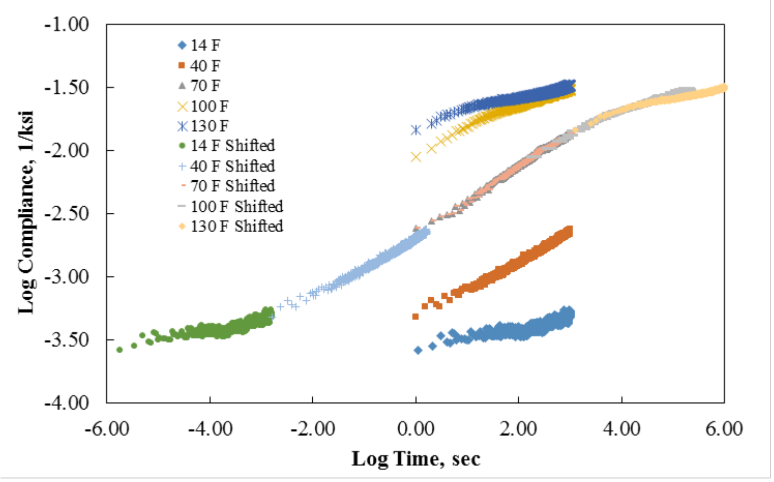

Figure 28 Development of creep compliance mastercurve.

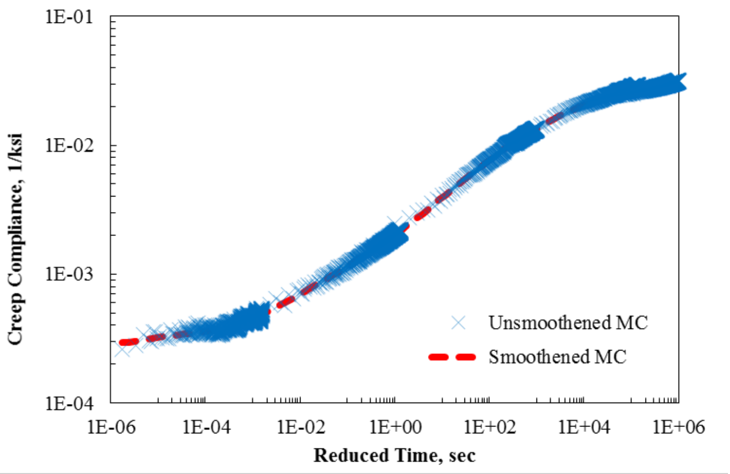

Figure 29 Unsmooth and smoothened creep compliance mastercurve.

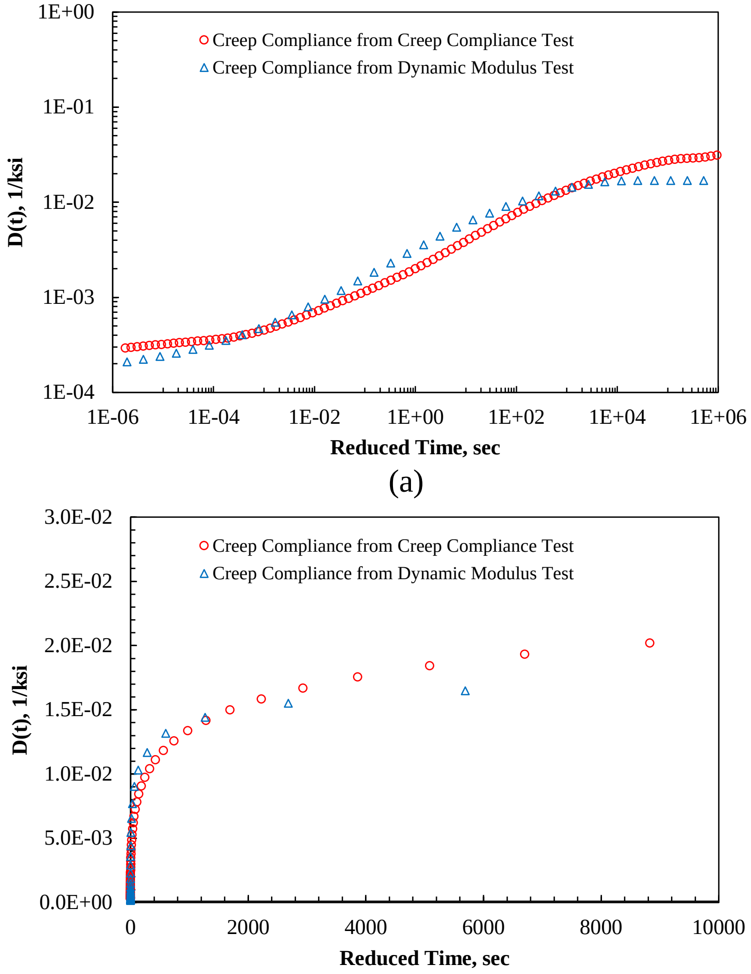

(a)

(b)

Figure 30 Laboratory tested and converted creep compliance functions: (a) in log-log scale, and (b) in normal scale (up to 10000 seconds reduced time).

Sample: SPIII PG70-22

Development of Creep Compliance Function

Figure 31 shows a typical uniaxial (compressive) creep test performed on a specimen of the AC mixture SPIII PG70-22 at a temperature of 14 °F. The figure shows the applied constant stress and the associated creep strain over 1000 seconds time period. Figure 32 shows the creep compliance as a function of time at different temperatures and the developed mastercurve by horizontally shifting the creep compliance data (known also as the application of time-temperature superposition principal). Figure 33 shows the unsmooth and smoothened creep compliance function.

Comparison of Tested and Converted Creep Compliance Functions for SPIII PG70-22 AC Mixture

Figures 34(a) and 34(b) show the creep compliance functions obtained from laboratory test and converted from *E** test data in log-log and normal scales, respectively. Observing the creep compliance functions found from two different source, it can be said that the numerical method of interconversion discussed earlier gives a good estimation of creep compliance considering the specimen to specimen variation as well as the limitation associated with laboratory testing. The difference in these two compliance functions is more toward the higher reduced time region.

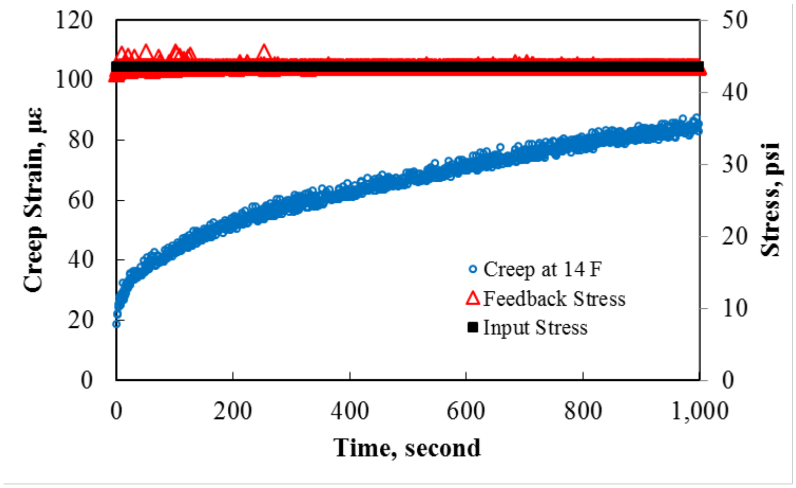

Figure 31 Typical uniaxial creep test at 14 °F.

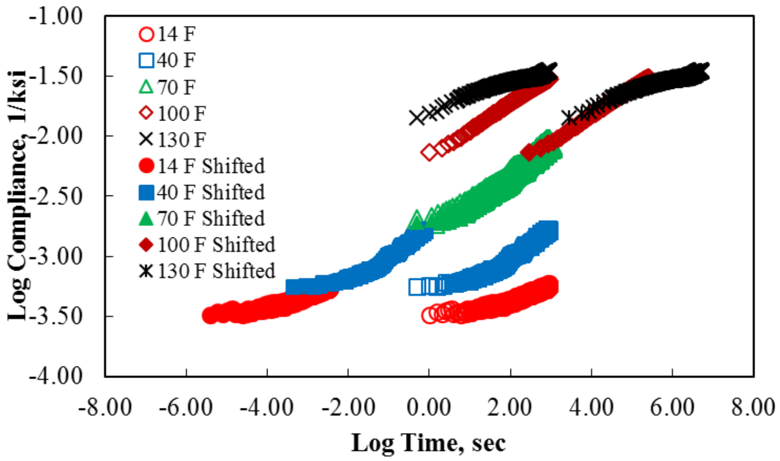

Figure 32 Development of creep compliance mastercurve.

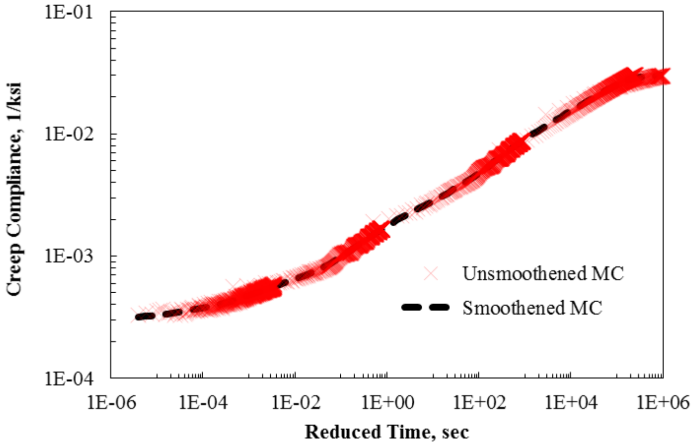

Figure 33 Unsmooth and smoothened creep compliance mastercurve.

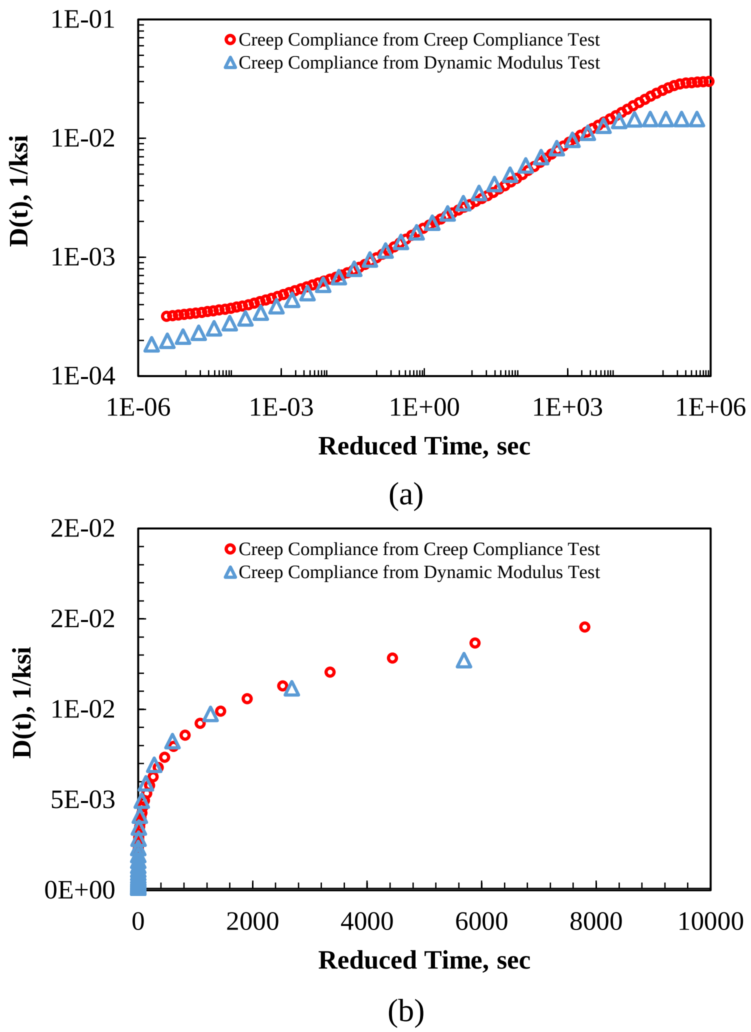

Figure 34 Laboratory tested and converted creep compliance functions: (a) in log-log scale, and (b) in normal scale (up to 10000 seconds reduced time).

Sample: SPIII PG76-22

Development of Creep Compliance Function

Figure 35 shows a typical uniaxial (compressive) creep test performed on a specimen of the AC mixture SPIII PG76-22 at a temperature of 14 °F. The figure shows the applied constant stress and the associated creep strain over 1000 seconds time period. Figure 36 shows the creep compliance as a function of time at different temperatures and the developed mastercurve by horizontally shifting the creep compliance data (known also as the application of time-temperature superposition principal). Figure 37 shows the unsmooth and smoothened creep compliance function.

Comparison of Tested and Converted Creep Compliance Functions for SPIII PG70-22 AC Mixture

Figures 38(a) and 38(b) show the creep compliance functions obtained from laboratory test and converted from *E** test data in log-log and normal scales, respectively. Observing the creep compliance functions found from two different source, it can be said that the numerical method of interconversion discussed earlier gives a good estimation of creep compliance considering the specimen to specimen variation as well as the limitation associated with laboratory testing. The difference in these two compliance functions is more toward the higher reduced time region.

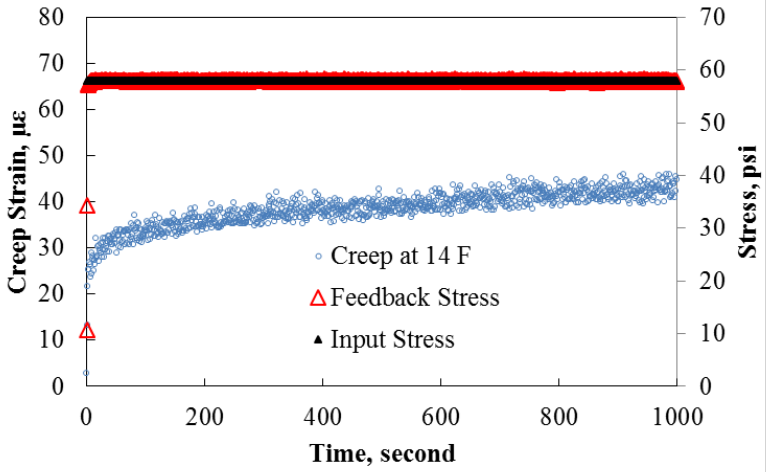

Figure 35 Uniaxial creep test at 14 °F test temperature.

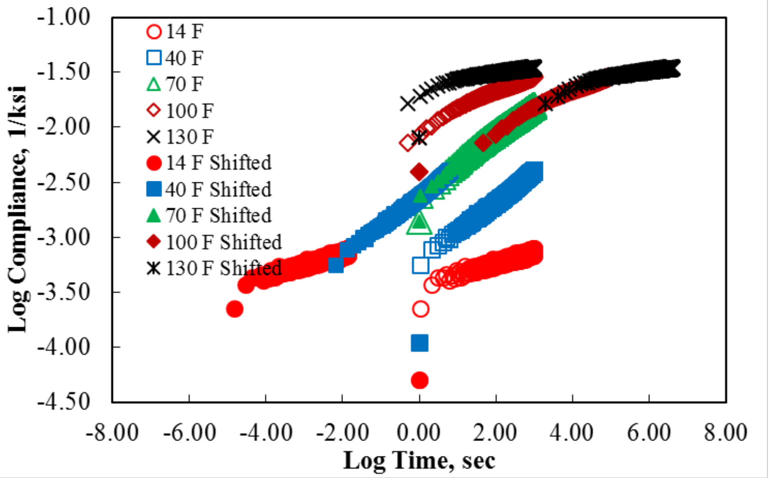

Figure 36 Development of Creep Compliance Mastercurve.

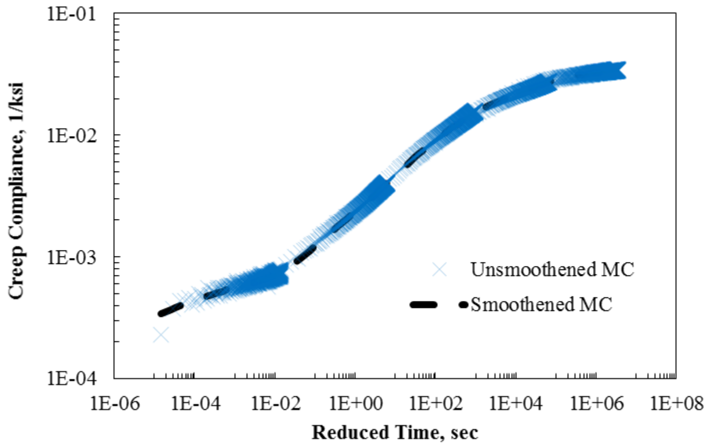

Figure 37 Unsmooth and smoothened Creep Compliance Mastercurve.

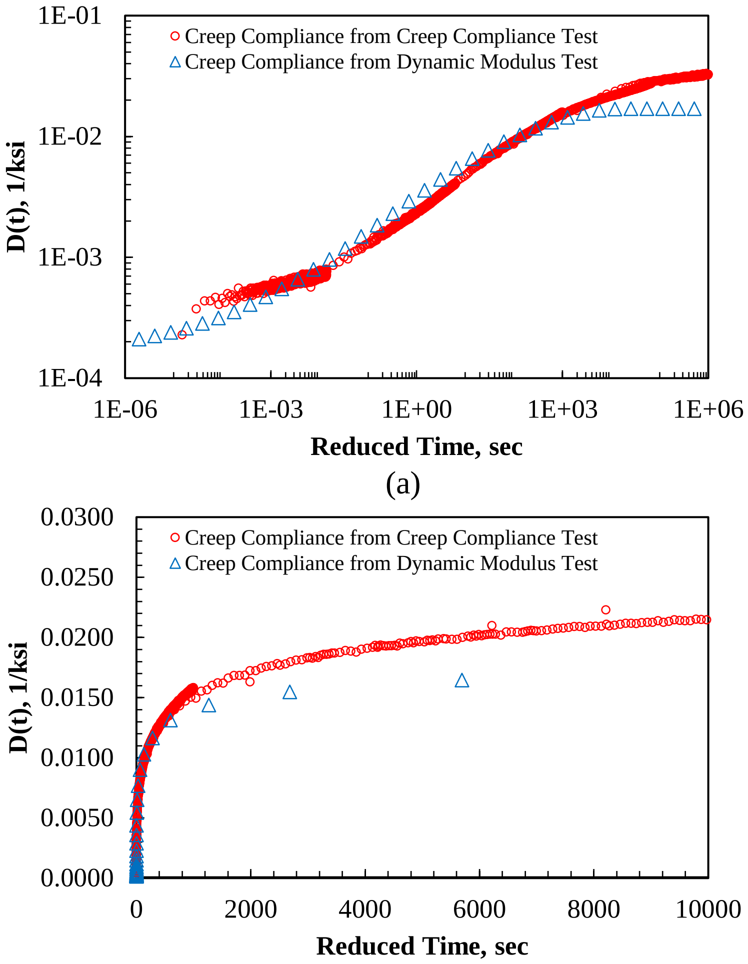

(a)

(b)

Figure 38 Laboratory tested and converted creep compliance functions: (a) in log-log scale, and (b) in normal scale (up to 10000 seconds reduced time).

Task 5: Relaxation Modulus Testing and Validation of Interconversion

Uniaxial Relaxation Modulus Test

Relaxation tests were conducted for 1000 seconds on each of the specimens at five different temperatures 14 °F, 40 °F, 70 °F, 100 °F, and 130 °F, starting from the lowest temperature and proceeding to the highest temperature. The applied total strains were 50 με, 50 με, 75 με, 100 με, and 150 με at temperatures 14 °F, 40 °F, 70 °F, 100 °F, and 130 °F, respectively. The maximum total strain limit was set to 150 με to avoid any possibility of leaving the linear viscoelastic range of the material. Finally, the relaxation modulus $E(t)$ was found by dividing the average relaxed stress of the two specimens by the input strain. Similar to creep compliance, the time temperature superposition principle was applied to develop average relaxation modulus mastercurve at 70 °F reference temperature. Again, to have a smoother representation of relaxation modulus, the developed mastercurve was smoothened using piecewise-polynomial fit.

Results

The AC mixtures were tested for relaxation modulus in the laboratory and the results are presented in the following sub-sections.

Sample: SPIV PG70-22

Development of Relaxation Modulus Function

Figure 39 shows a typical uniaxial (compressive) relaxation test performed on a specimen of the AC mixture SPIV PG70-22 at a temperature of 14 °F. The figure shows the applied constant strain and the associated relaxed stress over 1000 seconds time period. Figure 40 shows the relaxation modulus as a function of time at different temperatures and the developed mastercurve by horizontally shifting the relaxation modulus data (known also as the application of time-temperature superposition principal). Figure 41 shows the unsmooth and smoothened relaxation modulus function.

Comparison of Tested and Converted Relaxation Modulus Functions

Figures 42(a) and 42(b) show the relaxation modulus functions obtained from laboratory test and converted from E^* test data in log-log and normal scales, respectively. Observing these relaxation modulus functions found from two different sources, it can be said that the numerical method of interconversion discussed earlier gives a good estimation of relaxation modulus considering the specimen to specimen variation as well as the limitation associated with laboratory testing. The difference in these two modulus functions is more toward the lower reduced time region.

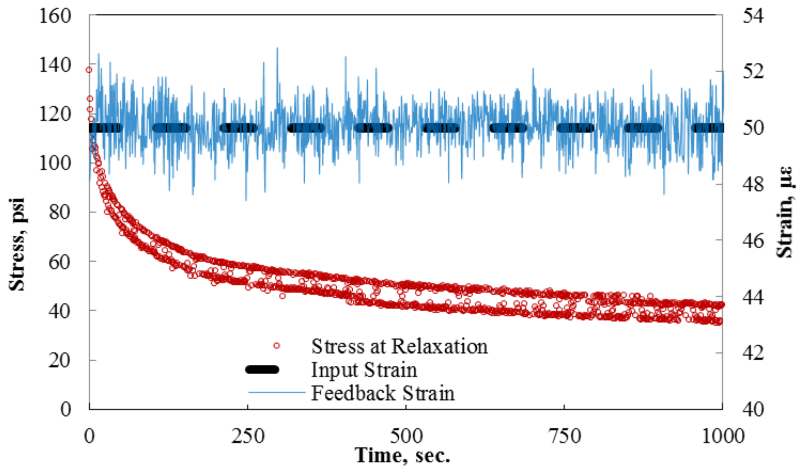

Figure 39 Typical uniaxial relaxation test.

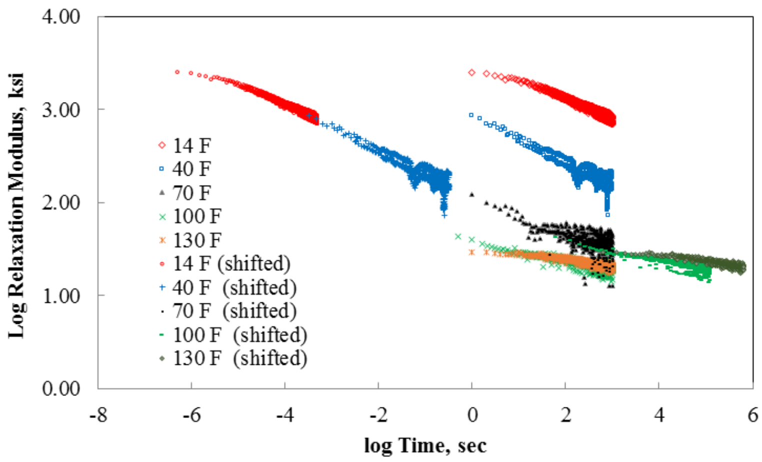

Figure 40 Development of relaxation modulus mastercurve.

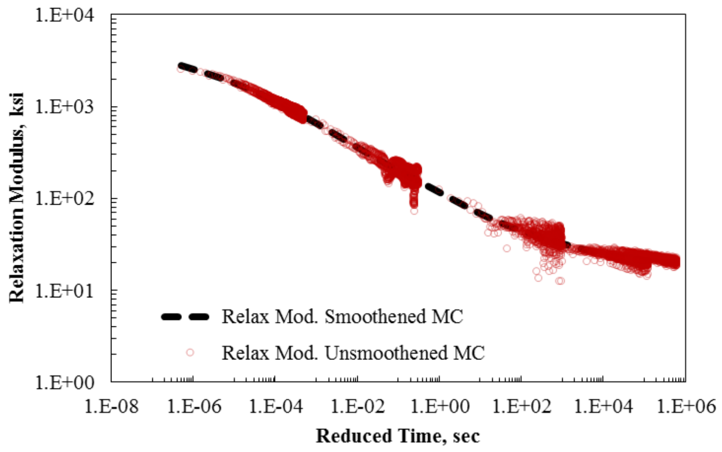

Figure 41 Unsmooth and smoothened relaxation modulus mastercurve.

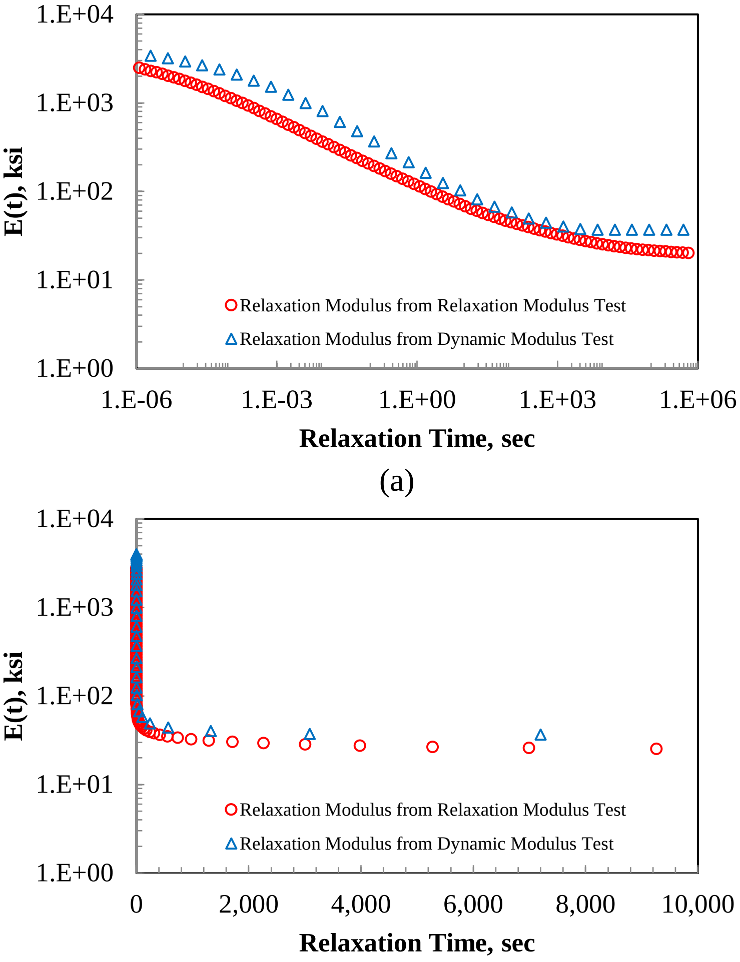

(a)

(b)

Figure 42 Laboratory tested and converted relaxation modulus functions: (a) in log-log scale, and (b) in semi-log scale (up to 10000 seconds reduced time).

Sample: SPIV PG76-22

Development of Relaxation Modulus Function

Figure 43 shows a typical uniaxial (compressive) relaxation test performed on a specimen of the AC mixture SPIV PG76-22 at a temperature of 14 °F. The figure shows the applied constant strain and the associated relaxed stress over 1000 seconds time period. Figure 44 shows the relaxation modulus as a function of time at different temperatures and the developed mastercurve by horizontally shifting the relaxation modulus data. Figure 45 shows the smoothened relaxation modulus function.

Comparison of Tested and Converted Relaxation Modulus Functions

Figures 46(a) and 46(b) show the relaxation modulus functions obtained from laboratory test and converted from *E** test data in log-log and normal scales, respectively. Observing these relaxation modulus functions found from two different sources, it can be said that the numerical method of interconversion discussed earlier gives a good estimation of relaxation modulus considering the specimen to specimen variation as well as the limitation associated with laboratory testing. The difference in these two modulus functions is more toward the lower reduced time region.

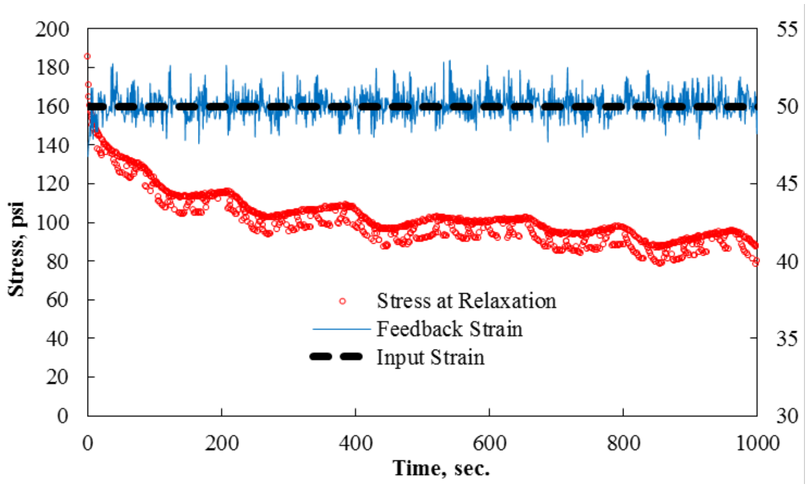

Figure 43 Typical uniaxial relaxation test.

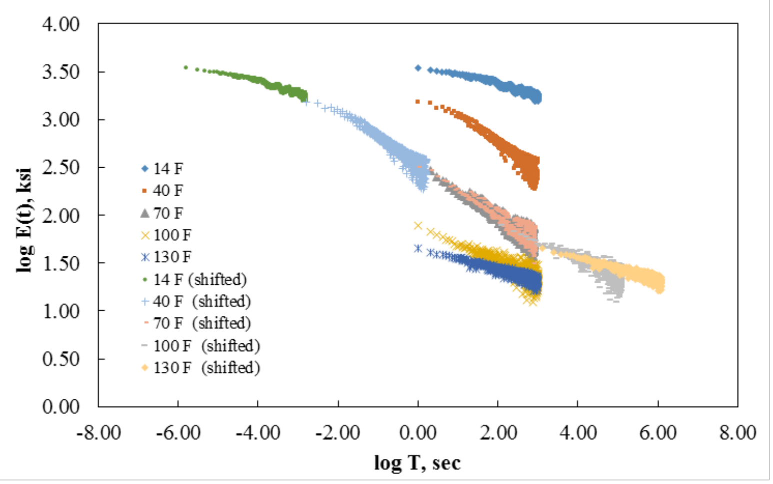

Figure 44 Development of relaxation modulus mastercurve.

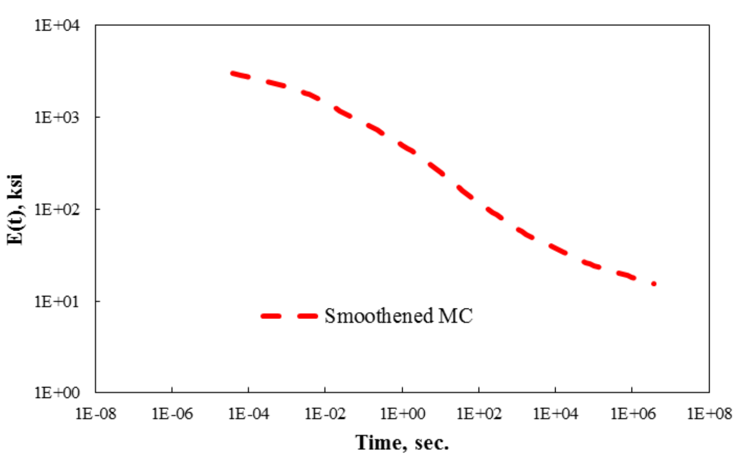

Figure 45 Smoothened relaxation modulus mastercurve.

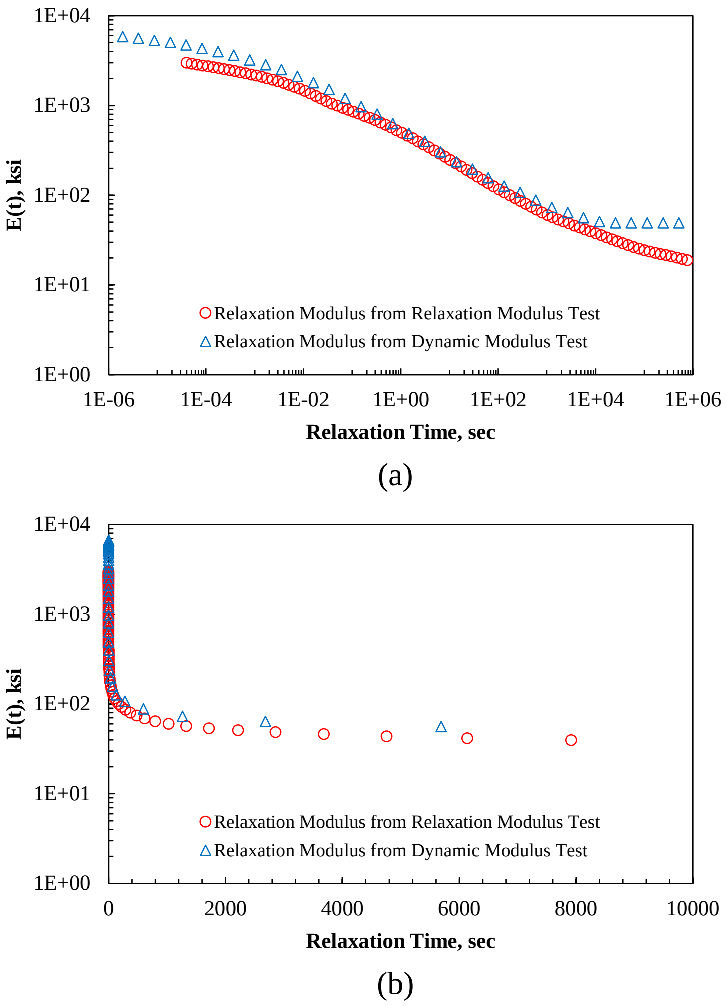

Figure 46 Laboratory tested and converted relaxation modulus functions: (a) in log-log scale, and (b) in semi-log scale (up to 10000 seconds reduced time).

Sample: SPIII PG70-22

Development of Relaxation Modulus Function

Figure 47 shows a typical uniaxial (compressive) relaxation test performed on a specimen of the AC mixture SPIII PG70-22 at a temperature of 14 °F. The figure shows the applied constant strain and the associated relaxed stress over 1000 seconds time period. Figure 48 shows the relaxation modulus as a function of time at different temperatures and the developed mastercurve by horizontally shifting the relaxation modulus data. Figure 49 shows the smoothened relaxation modulus function.

Comparison of Tested and Converted Relaxation Modulus Functions

Figures 50(a) and 50(b) show the relaxation modulus functions obtained from laboratory test and converted from *E** test data in log-log and normal scales, respectively. Observing these relaxation modulus functions found from two different sources, it can be said that the numerical method of interconversion discussed earlier gives a good estimation of relaxation modulus considering the specimen to specimen variation as well as the limitation associated with laboratory testing. The difference in these two modulus functions is more toward the lower reduced time region.

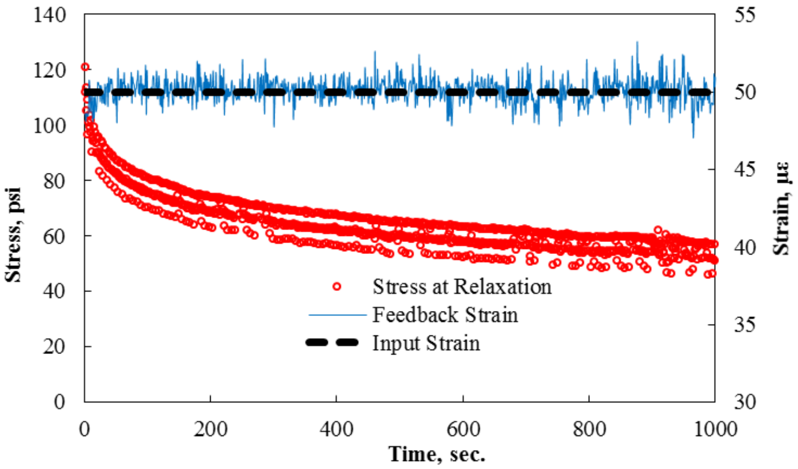

Figure 47 Typical uniaxial relaxation test.

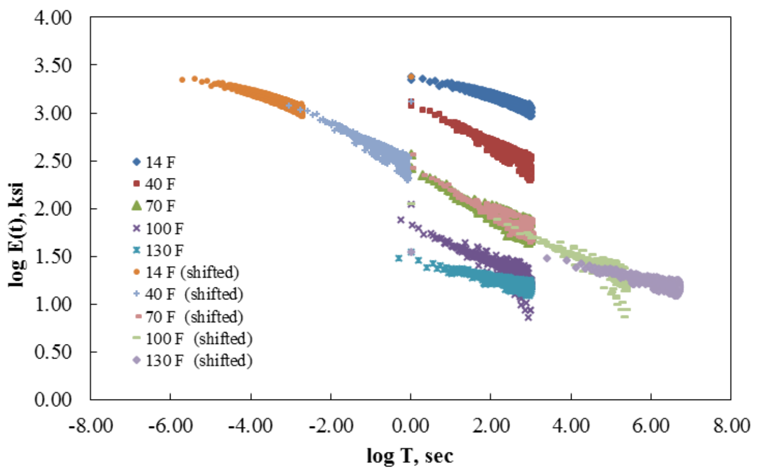

Figure 48 Development of relaxation modulus mastercurve.

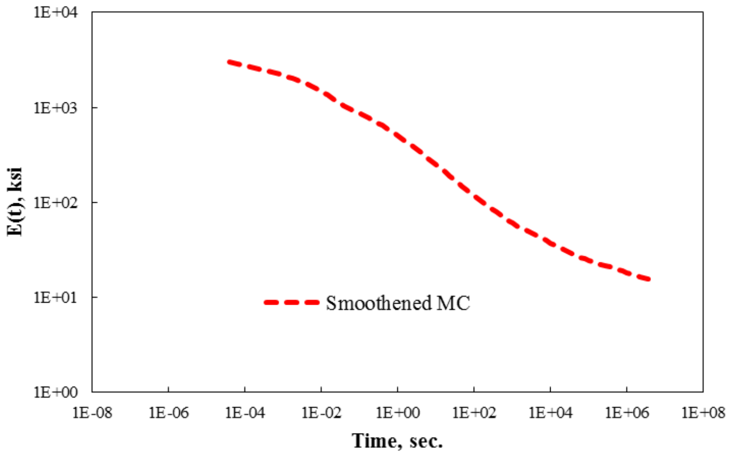

Figure 49 Smoothened relaxation modulus mastercurve.

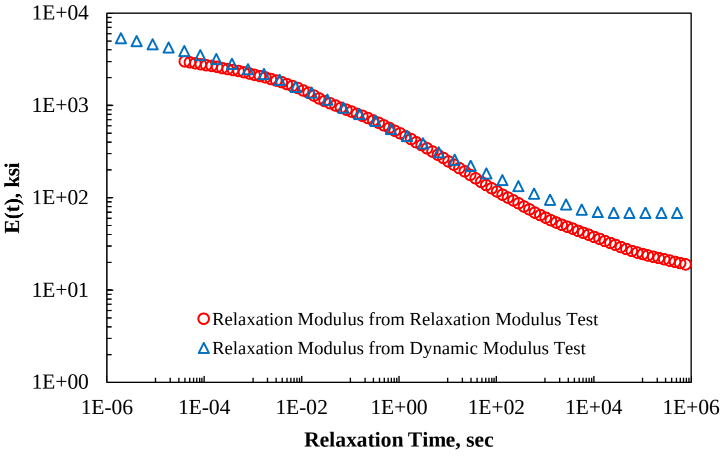

(a)

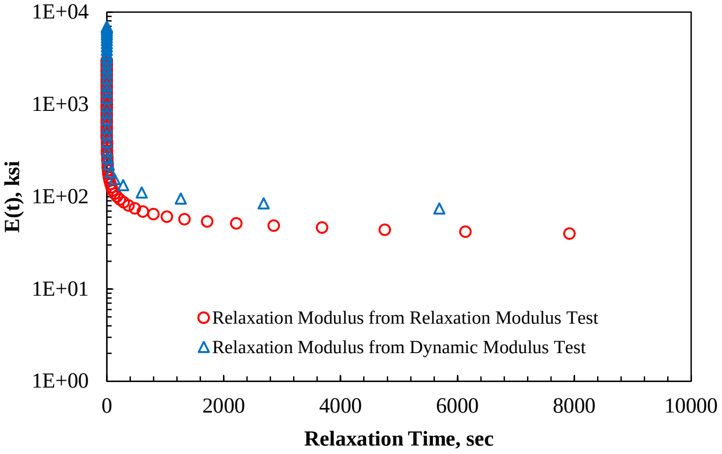

(b)

Figure 50 Laboratory tested and converted relaxation modulus functions: (a) in log-log scale, and (b) in semi-log scale (up to 10000 seconds reduced time).

Sample: SPIII PG76-22

Development of Relaxation Modulus Function

Figure 51 shows a typical uniaxial (compressive) relaxation test performed on a specimen of the AC mixture SPIII PG76-22 at a temperature of 14 °F. The figure shows the applied constant strain and the associated relaxed stress over 1000 seconds time period. Figure 52 shows the relaxation modulus as a function of time at different temperatures and the developed mastercurve by horizontally shifting the relaxation modulus data. Figure 53 shows the smoothened relaxation modulus function.

Comparison of Tested and Converted Relaxation Modulus Functions

Figures 54(a) and 54(b) show the relaxation modulus functions obtained from laboratory test and converted from *E** test data in log-log and normal scales, respectively. Observing these relaxation modulus functions found from two different sources, it can be said that the numerical method of interconversion discussed earlier gives a good estimation of relaxation modulus considering the specimen to specimen variation as well as the limitation associated with laboratory testing. The difference in these two modulus functions is more toward the lower reduced time region.

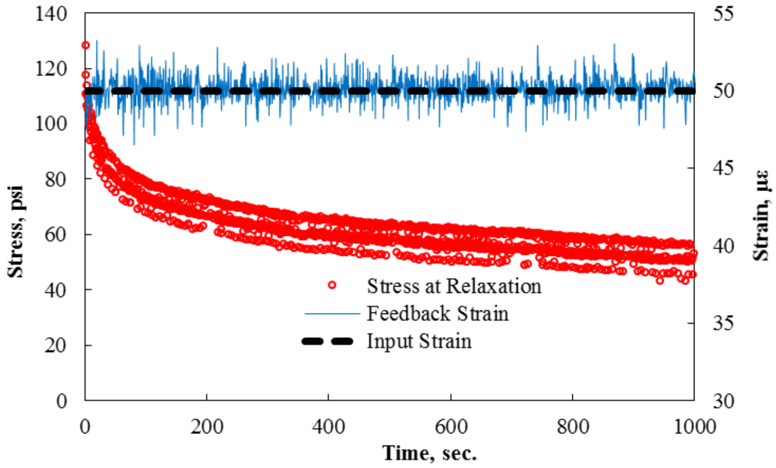

Figure 51 Typical uniaxial relaxation test.

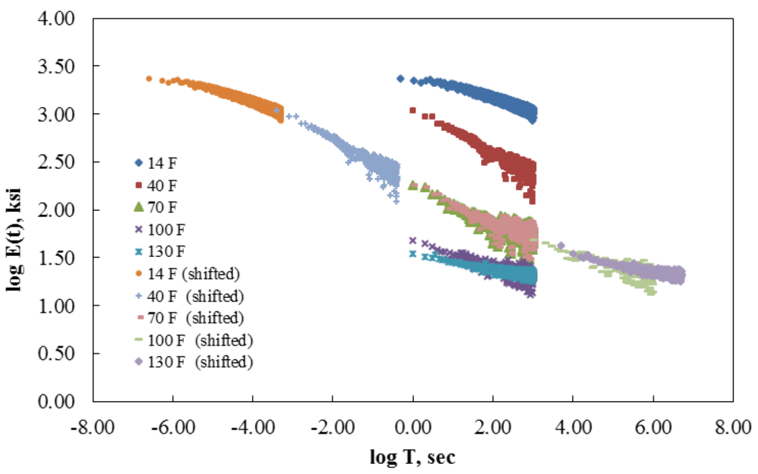

Figure 52 Development of relaxation modulus mastercurve.

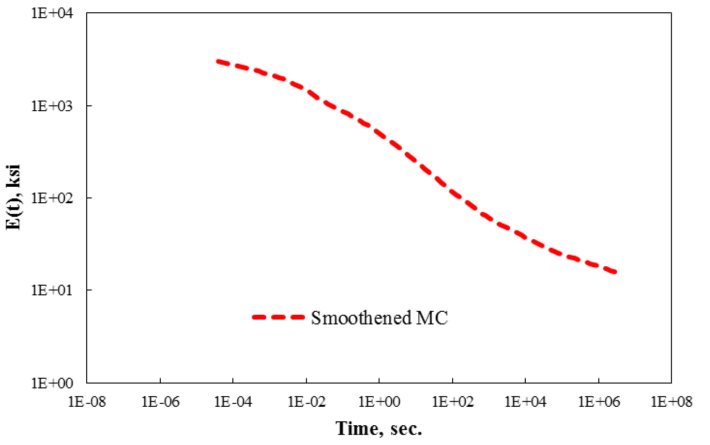

Figure 53 Smoothened relaxation modulus mastercurve.

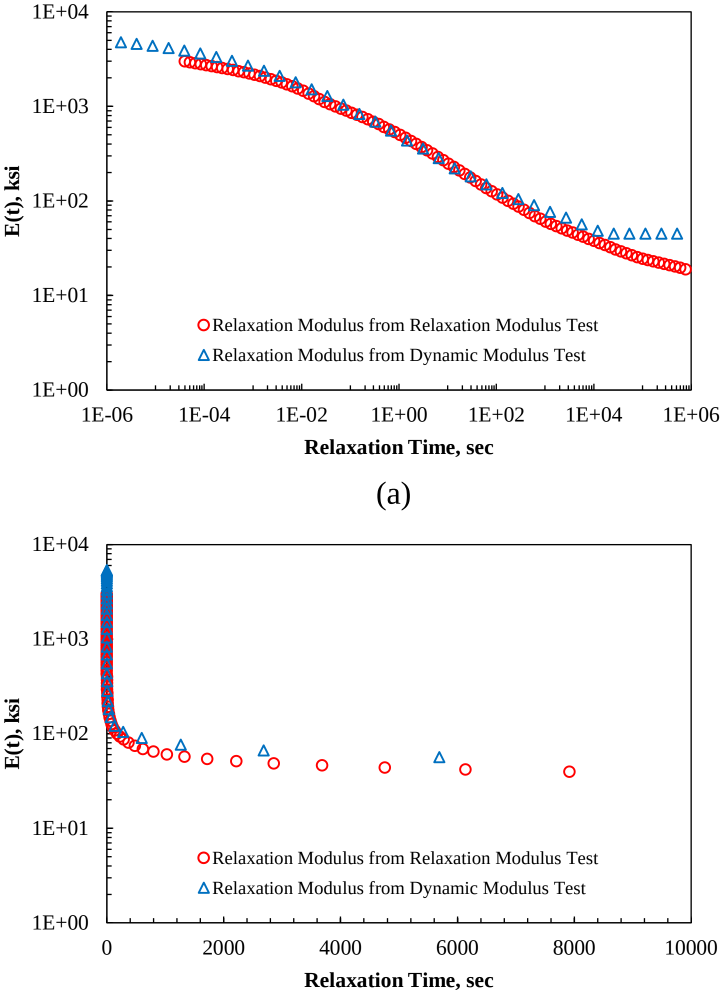

(a)

(b)

Figure 54 Laboratory tested and converted relaxation modulus functions: (a) in log-log scale, and (b) in semi-log scale (up to 10000 seconds reduced time).

STATISTICAL EVALUATION

To check if the $D(t)$ and $E(t)$ functions found from the two different sources are significantly different or not, statistical t-tests and single factor analyses of variances (ANOVA) were conducted in this study. The α-value in these both type of analysis is considered to be 0.05. The t-tests in case of both $D(t)$ and $E(t)$ showed the p-value to be greater than $\alpha = 0.05$, which infers that, at 95% confidence level the there is no significant difference in means is observed for the $E(t)$ and $D(t)$ functions found from direct laboratory tests and interconverted from dynamic modulus or storage modulus.

The single factor ANOVA analyses showed that the F-values are well below the critical F-value ($F_{critical}$) with p-values greater than $\alpha = 0.05$ for both $D(t)$ and $E(t)$ functions found from two different sources. This also indicates that the $D(t)$ and $E(t)$ functions found from the two different sources are not significantly different.

CONCLUSIONS

In this study, an exact numerical approach to convert frequency domain complex modulus to time domain relaxation modulus and creep compliance is presented and validated by laboratory tests in case of asphalt concrete. Based on the analyses and results it can be said that the numerical method reviewed in this study is proved to be applicable in case of asphalt concrete to interconvert frequency domain modulus to time domain modulus and compliance. Although, the converted and tested relaxation modulus are not found in good agreement, considering specimen to specimen variation and common laboratory limitations associated with the tests, the method can be well used for application in asphalt industry.

REFERENCES

[1] MEPDG, 2004, Guide for Mechanistic-Empirical Design of New and Rehabilited Pavement Structure. NCHRP Final Report.

[2] Hopkins, I. L., and Hamming, R. W., 1957, "On creep and relaxation," *Journal of Applied Physics*, Vol. 28 (8), pp. 906-909.

[3] Knoff, W. F., and Hopkins, I. L., 1972, "An improved numerical interconversion for creep compliance and relaxation modulus," *Journal of Applied Polymer Science*, Vol. 16, pp. 2963-2972.

[4] Baumgaertel, M., and Winter, H. H., 1989, "Determination of discrete relaxation and retardation time spectra from dynamic mechanical data," *Rheologica Acta*, Vol. 28, pp. 511-519.

[5] Mead, D. W., 1998, "Numerical interconversion of linear viscoelastic material functions," *Journal of Rheology*, Vol. 38, pp. 1769-1795.

[6] Schapery, R. A., and Park, S. W., 1998, "Methods of interconversion between linear viscoelastic material functions. Part II – An approximate analytical method," *International Journal of Solids and Structures*, Vol. 36, pp. 1677-1699.

[7] Ramkumar, D. H. S., Caruthers, J. M., Mavridis, H., Shroff, R., 1997, "Computation of the linear viscoelastic relaxation spectrum from experimental data," *Journal of Applied Polymer Science*, Vol. 64, pp. 2177-2789.

[8] Park, S. W., and Schapery, R. A., 1999, "Methods of interconversion between linear viscoelastic material functions, Part I – a numerical method based on Prony series," *International Journal of Solids and Structures*, Vol. 3, pp. 1653-1675.

[9] Mun, S., Chehab, G. R., and Kim, Y. R., 2007, "Determination of Time-domain Viscoelastic Functions using Optimized Interconversion Techniques," *Road Materials and Pavement Design*, Vol. 8, pp. 351-365.

[10] Park, S. W., and Kim, Y. R., 1999, "Interconversion between Relaxation Modulus and Creep Compliance for Viscoelastic Solids," *Journal of Materials in Civil Engineering*, Vol. 11, pp. 76-82.

[11] Daniel, J. S., Kim, Y. R., and Lee, H., 2007, "Effects of Aging on Viscoelastic Properties of Asphalt-Aggregate Mixture," *Transportation Research Record: Journal of the Transportation Research Board*, No. 1630, Washington, D.C., pp. 21-27.

[12] Kim, Y. R., and Lee, Y. C., 1995, "Interrelationships among Stiffnesses of Asphalt-Aggregate Mixtures," *Journal of the Association of Asphalt Paving Technologists*, Vol. 64, pp. 575-609.

[13] AASHTO T 209, 2009, "Theoretical Maximum Specific Gravity and Density of Hot-Mix Asphalt Paving Mixtures," *Standard Specifications for Transportation Materials and Methods of Sampling and Testing*, AASHTO, Washington D.C.

[14] AASHTO T 342, 2011, "Standard Method of Test for Determining Dynamic Modulus of Hot-Mix Asphalt Concrete Mixtures," *Standard Specifications for Transportation Materials and Methods of Sampling and Testing*, AASHTO, Washington D.C.

[15] Park, S. W., and Kim, Y. R., 2001, "Fitting Prony-Series Viscoelastic Models with Power-Law Presmoothing," *Journal of Materials in Civil Engineering*, Vol. 13, pp. 26-32.

[16] Rahman, A. S. M. A., Islam, M. R., and Tarefder, R. A., 2016, "Modifying the Viscosity based Witczak Model and Developing Phase Angle Predictive Model for New Mexico's

Superpave Mixes," *95th Annual Meeting of Transportation Research Board*, Washington D.C., United States, Paper No. 16-3180.